

AD-A199 874

UDR-TR-88-94

AFOSR-TR- 88-1020

(2)

FINAL REPORT ON THE INTERFACE STABILITY  
BETWEEN TWO GAS STREAMS OF DIFFERENT DENSITY  
IN A CURVED FLOW

J.E. Minardi  
M.P. Skomrock  
Hans von Ohain  
M.O. Lawson  
L.I. Boehman

UNIVERSITY OF DAYTON  
RESEARCH INSTITUTE  
DAYTON, OHIO 45469

DTIC  
ELECTED  
OCT 06 1988  
S H D

DISTRIBUTION STATEMENT A

Approved for public release;  
Distribution Unlimited

88 10 5 289

UNCLAS. IED

SECURITY CLASSIFICATION OF THIS PAGE

## REPORT DOCUMENTATION PAGE

1a. REPORT SECURITY CLASSIFICATION <del>UNCLASSIFIED</del>		1b. RESTRICTIVE MARKINGS										
2a. SECURITY CLASSIFICATION AUTHORITY		3. DISTRIBUTION/AVAILABILITY OF REPORT <b>APPROVED FOR PUBLIC RELEASE</b> <b>DISTRIBUTION IS UNLIMITED</b>										
2b. DECLASSIFICATION/DOWNGRADING SCHEDULE		4. PERFORMING ORGANIZATION REPORT NUMBER(S) <b>AFOSR 86-1020</b>										
5. MONITORING ORGANIZATION REPORT NUMBER(S)												
6a. NAME OF PERFORMING ORGANIZATION <b>UNIVERSITY OF DAYTON</b>	6b. OFFICE SYMBOL (if applicable)	7a. NAME OF MONITORING ORGANIZATION <b>AFOSR/NA</b>										
6c. ADDRESS (City, State, and ZIP Code) <b>AEROSPACE MECHANICS DIVISION 300 COLLEGE PARK, DAYTON OH 45469</b>		7b. ADDRESS (City, State, and ZIP Code) <b>BUILDING 410 BOLLING AFB, DC 20332-6448</b>										
8a. NAME OF FUNDING/SPONSORING ORGANIZATION <b>AFOSR</b>	8b. OFFICE SYMBOL (if applicable) <b>NA</b>	9. PROCUREMENT INSTRUMENT IDENTIFICATION NUMBER <b>AFOSR 86-0137</b>										
8c. ADDRESS (City, State, and ZIP Code) <b>BUILDING 410 BOLLING AFB, DC 20332-6448</b>		10. SOURCE OF FUNDING NUMBERS <table border="1"><tr><td>PROGRAM ELEMENT NO <b>61102F</b></td><td>PROJECT NO. <b>2307</b></td><td>TASK NO. <b>A 4</b></td><td>WORK UNIT ACCESSION NO</td></tr></table>		PROGRAM ELEMENT NO <b>61102F</b>	PROJECT NO. <b>2307</b>	TASK NO. <b>A 4</b>	WORK UNIT ACCESSION NO					
PROGRAM ELEMENT NO <b>61102F</b>	PROJECT NO. <b>2307</b>	TASK NO. <b>A 4</b>	WORK UNIT ACCESSION NO									
11. TITLE (Include Security Classification) <b>(U) INTERFACE STABILITY BETWEEN TWO GAS STREAMS of Different Density</b>												
12. PERSONAL AUTHOR(S) <b>J. E. MINARDI</b>		13a. TYPE OF REPORT <b>FINAL</b>										
13b. TIME COVERED FROM <u>1 Apr 86</u> TO <u>31 Mar 88</u>		14. DATE OF REPORT (Year, Month, Day) <b>AUG 1988</b>										
15. PAGE COUNT <b>58</b>												
16. SUPPLEMENTARY NOTATION												
17. COSATI CODES <table border="1"><tr><th>FIELD</th><th>GROUP</th><th>SUB-GROUP</th></tr><tr><td></td><td></td><td></td></tr><tr><td></td><td></td><td></td></tr></table>		FIELD	GROUP	SUB-GROUP							18. SUBJECT TERMS (Continue on reverse if necessary and identify by block number) <b>TURBINE COOLING, TURBULENT FLOW, MIXING</b>	
FIELD	GROUP	SUB-GROUP										
19. ABSTRACT (Continue on reverse if necessary and identify by block number) <b>A novel cooling concept applicable to small turbine engines is discussed. The concept involves co-flowing streams within the turbine blade passage: one cold and one hot. Fundamental studies of turbulent flow in curved channels of two streams of different total temperatures and pressures are discussed.</b>												
20. DISTRIBUTION/AVAILABILITY OF ABSTRACT <input type="checkbox"/> UNCLASSIFIED/UNLIMITED <input checked="" type="checkbox"/> SAME AS RPT <input type="checkbox"/> DTIC USERS		21. ABSTRACT SECURITY CLASSIFICATION <b>UNCLASSIFIED</b>										
22a. NAME OF RESPONSIBLE INDIVIDUAL <b>HENRY E. HELIN</b>		22b. TELEPHONE (Include Area Code) <b>202-767-0471</b>	22c. OFFICE SYMBOL <b>AFOSR/NA</b>									

FINAL REPORT ON THE INTERFACE STABILITY  
BETWEEN TWO GAS STREAMS OF DIFFERENT DENSITY  
IN A CURVED FLOW

J.E. Minardi  
M.P. Skomrock  
Hans von Ohain  
M.O. Lawson  
L.I. Boehman

UNIVERSITY OF DAYTON  
RESEARCH INSTITUTE  
DAYTON, OHIO 45469

## FOREWORD

The work reported herein was performed for the Air Force Office of Scientific Research (AFOSR) under grant AFOSR-86-0137. Dr. James D. Wilson and Capt. H. Helin were the Program Managers. This report covers the work from 1 April 1986 to 31 March 1988.

The authors wish to thank Mr. Tom Prevish for his help in the program. The authors would especially like to thank Mrs. Karen Reynolds for her assistance in preparation of this report.



Accession For	
NTIS GRA&I	<input checked="" type="checkbox"/>
DTIC TAB	<input type="checkbox"/>
Unannounced	<input type="checkbox"/>
Justification	
By _____	
Distribution/	
Availability Codes	
Avail and/or	
Dist	Special
A-1	

## ABSTRACT

Performance trends in gas turbine engine designs have led to higher turbine inlet temperatures. These more severe temperature conditions require novel cooling methods for small turbines as well as novel heat/oxidation resistant materials. A ~~Novel cooling concept especially applicable to small turbines is briefly described. The concept~~ involves co-flowing streams within the turbine blade passage: one cold and one hot. This concept, referred to as the Radiax Turbine, provides for strong blade cooling even in very small turbines where traditional cooling approaches cannot be used. However, fundamental studies of turbulent flow in curved channels of two streams of different total pressure and temperature are required to provide the basic information needed in understanding this co-flowing streams in a curved channel. Studies of the literature, have shown that the technical importance of the research results would not be limited to turbine rotor cooling but would have wide engineering application.

This report covers the design of an experimental apparatus that will be used for investigating the interface stability between two gas streams of different densities in a curved flow and reports on flow visualization studies performed with the apparatus. More complete measurements will be reported later in Capt. Skomrock's dissertation. Several types of instability are possible in these curved mixing layers and they are discussed in the report.

## TABLE OF CONTENTS

SECTION	PAGE
1 INTRODUCTION	1
2 TECHNICAL APPROACH	5
2.1 EXPERIMENTAL APPROACH	5
2.1.1 Historical Review	5
2.1.2 Discussion of Experimental Approach	10
2.1.2.1 Characteristics of the Flow Path Configuration	15
2.1.2.2 The Range of Flow Conditions	16
3 EXPERIMENTAL APPARATUS	20
4 RESULTS	30
5 CONCLUSIONS	47
6 RECOMMENDATIONS	49
7 REFERENCES	50

## LIST OF ILLUSTRATIONS

FIGURES		PAGE
1	Schematic of Aircooled Radiax Turbine.	2
2	Schematic of the Curved Flow Channel. Traverses in the Radial and Spanwise Directions will be made at seven stations spaced at $\Delta\phi = 15^\circ$ .	6
3	Schematic Profile of Ventilated Wall Jet (from Reference 14).	9
4	Schematic Profile of a Ventilated Jet of a Circular Arc (from Reference 15).	9
5	Schematic Diagram of Test Rig from Reference 16. All Dimensions in Centimeters.	9
6	Stability Regimes for Curved Flows.	13
7	Schematic View of the Experimental Apparatus.	17
8	Experimental Apparatus Layout with the Various Elements Identified by Numbers.	21
9	Electric Heaters Used to Heat the Incoming Air.	23
10	Stilling Chamber and Splitter Plate.	24
11	The hollow Splitter Plate Extends Beyond the Exit of the Stilling Chamber.	25
12	End View of Clear Plastic Side Plates Showing the Boundary Layer Suction Groves.	26
13	Transition Section Attached to the Curved Flow Channel.	27
14	A Mount Could be Provided to Allow the Stilling Chamber and the Curved Channel to Pivot About the Center of the Channel.	28
15.A	Air at equal densities, various velocities and dynamic pressures. Set 1 (a,b,c, and d).	34
15.B	Air at equal densities, various velocities and dynamic pressures. Set 1 (e,f,g, and h).	35
16.A	Air at equal densities and dynamic pressures with various velocities. Set 2 (a,b,c, and d).	36

FIGURES	PAGE
17.A      High speed flash of air-air at equal densities. Set 3 (a,b,c, and d).	37
17.B      High speed flash of air-air at equal densities. Set 3 (e,f, and g).	38
18.A      Air at various densities, velocities, and dynamic pressures. Set 4 (a,b,c, and d).	39
18.B      Air at various densities, velocities, and dynamic pressures. Set 4 (e,f,g, and h).	40
18.C      Air at various densities, velocities, and dynamic pressures. Set 4 (i,j,k, and l).	41
18.D      Air at various densities, velocities, and dynamic pressures. Set 4 (m,n,o, and p).	42
19.A      Air at equal dynamic pressures, various velocities and densities. Set 5 (a,b,c, and d).	43
19.B      Air at equal dynamic pressures, various velocities and densities. Set 5 (e,f,g, and h).	44
20.A      Air at equal velocities, various dynamic pressures and densities. Set 6 (a,b,c, and d).	45
20.B      Air at equal velocities, various dynamic pressures and densities. Set 6 (e,f).	46

LIST OF TABLES

TABLE	PAGE
1 TEST COMBINATIONS OF TOTAL PRESSURE AND STATIC DENSITY	18

UNIVERSITY OF DAYTON  
RESEARCH INSTITUTE  
DAYTON, OHIO 45469

SECTION 1

INTRODUCTION

Recent trends in small gas turbines as in larger turbines have moved toward higher thermal efficiencies. This means greater pressure ratios, 30:1 and beyond, and correspondingly higher compressor exit temperatures like 1,400 degrees R or greater. As a consequence, turbine inlet temperatures must also rise dramatically. These conditions necessitate intense blade cooling methods or new heat/oxidation resistant materials. More than likely, a combination of both cooling and materials will be required to push the state of the art to the highest possible levels.

In large gas turbines, the techniques of hollow blades employing combined internal heat transfer and film cooling methods are very advanced. However, for small gas turbine engines having thrust levels of about 1,000 pounds or less, these methods are not applicable. Hence, for small gas turbine engines, novel, very intense blade cooling methods, which cause only a very small decrease in equivalent turbine efficiency, are needed.

In response to this need, the University of Dayton Research Institute has developed a cooling concept which we refer to as a Radiax turbine. A schematic of the Radiax turbine is shown in Figure 1. The Radiax turbine is especially suited to the small turbine application since it does not need any internal cooling passages. Rather, two different entries to the turbine blades are provided as shown in Figure 1. The hot gas enters the turbine blade at the top (indicated by the thick arrows) and the

Aircooled Radiax Turbine:

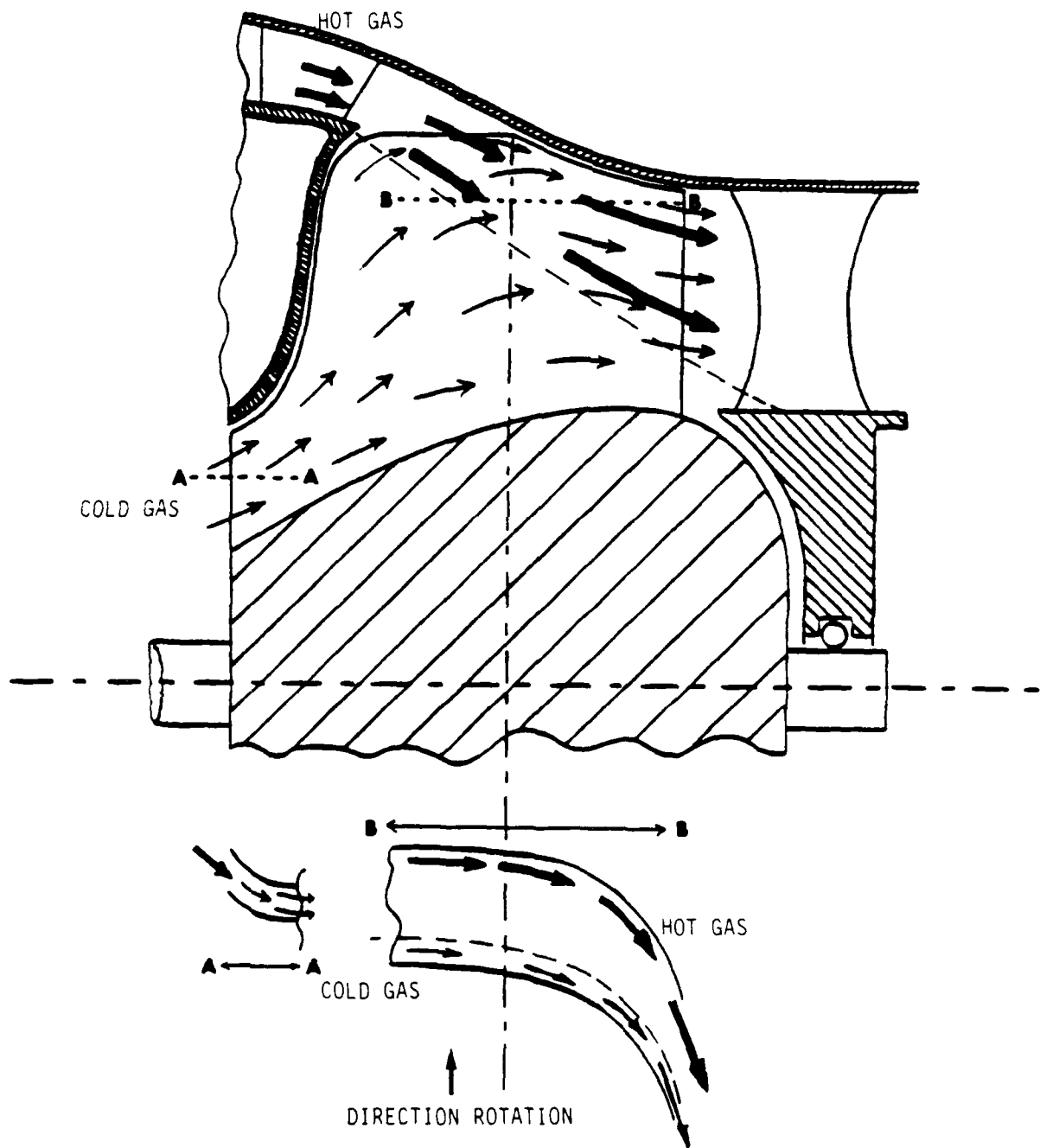


Figure 1. Schematic of Aircooled Radiax Turbine

cold gas at the bottom left (indicated by the thin arrows). As indicated in Figure 1 by section A-A, the leading edge where the cold flow enters, the wheel acts as a compressor inlet and compresses the cold gas entering the turbine section. The hot gas, on the other hand, enters the turbine wheel at the top as in a radial flow turbine, but with a strong axial component. Both flows stay separated and coexist in the turbine section as shown in section B-B of Figure 1. The hot gas goes to the pressure side of the blade and the cold gas goes to the suction side of the blade. Thus, each blade has hot gas on one side and cold gas on the other. This condition provides a strong cooling effect to the blade from hub to tip without reducing the turbine efficiency to an unacceptable level.

The technical objectives of the Radiax turbine with its "dual stream" blade cooling method are:

- a. utilization of solid blades cooled on one blade side;
- b. intense cooling from blade-leading to trailing edge;
- c. efficient cooling corresponding to small performance penalty in comparison to uncooled blades (because the cooling gas does not flow through a stator or through small internal passages; and
- d. exploitation of the inherent advantages of solid aircooled blades:
  - structural simplicity, and low manufacturing cost;
  - excellent suitability for:
    - smallest size high performance gas turbine;
    - application of novel, high temperature materials; and

- application of oxidation-protection layer, and thermal barrier materials on the hot blade side exposed to the hot gas stream.

In order to develop the understanding required to meet these technical objectives, the UDRI has undertaken a research program designed to gain understanding of a basic nature for curved flows of two gas streams with different total pressures and temperatures. The technical importance of this research will not be limited to turbine rotor cooling. Other applications such as stationary vane cooling, combustor wall cooling, and many other wall cooling applications will benefit from the proposed research.

The basic research objectives are:

- a. understanding of mixing phenomena between two co-flowing streams of different total pressure and temperature in the presence of inertial force fields within the blade passages
  - centrifugal forces (blade passage curvature) and
  - Coriolis forces (radial flow components; not included in the present research);
- b. flow stratification: formation of hot and cold streams within the blade passages;
- c. conditions for interface stability/instability; and
- d. mixing along interface in a curved channel (under stable and unstable conditions).

A discussion of the technical approach is given in the next section.

## SECTION 2

### TECHNICAL APPROACH

The study involves an experimental approach that is briefly discussed in this section.

#### 2.1 EXPERIMENTAL APPROACH

Detailed measurements within a passage of a rotor system would not be practical until a basic understanding of the flowfield is developed. Further, at this time we plan to look at a channel flow with curvature and two co-flowing air streams of different temperature and velocity (see Figure 2). The research is focused on the interface between the two gas streams of different temperature and velocity flowing through a curved two-dimensional flow channel. Of specific importance are the physical conditions which govern:

- stability/instability of the interface between the two flows;
- entrainment and mixing phenomena at the shear layer;
- occurrence and history of large vortices.

It is instructive to first briefly review related research efforts and determine how the interest in the phenomena evolved historically.

##### 2.1.1 Historical Review

Bradshaw<sup>1</sup>, in a paper discussing the analogy between curvature and buoyancy in turbulent flow, also considers rotating flows. He noted, ". . . one would expect less difference between rotation and curvature than between curvature and buoyancy." Therefore, since we agree with this assessment, we chose to investigate experimentally the flow in the curved two-dimensional channel shown in Figure 2.

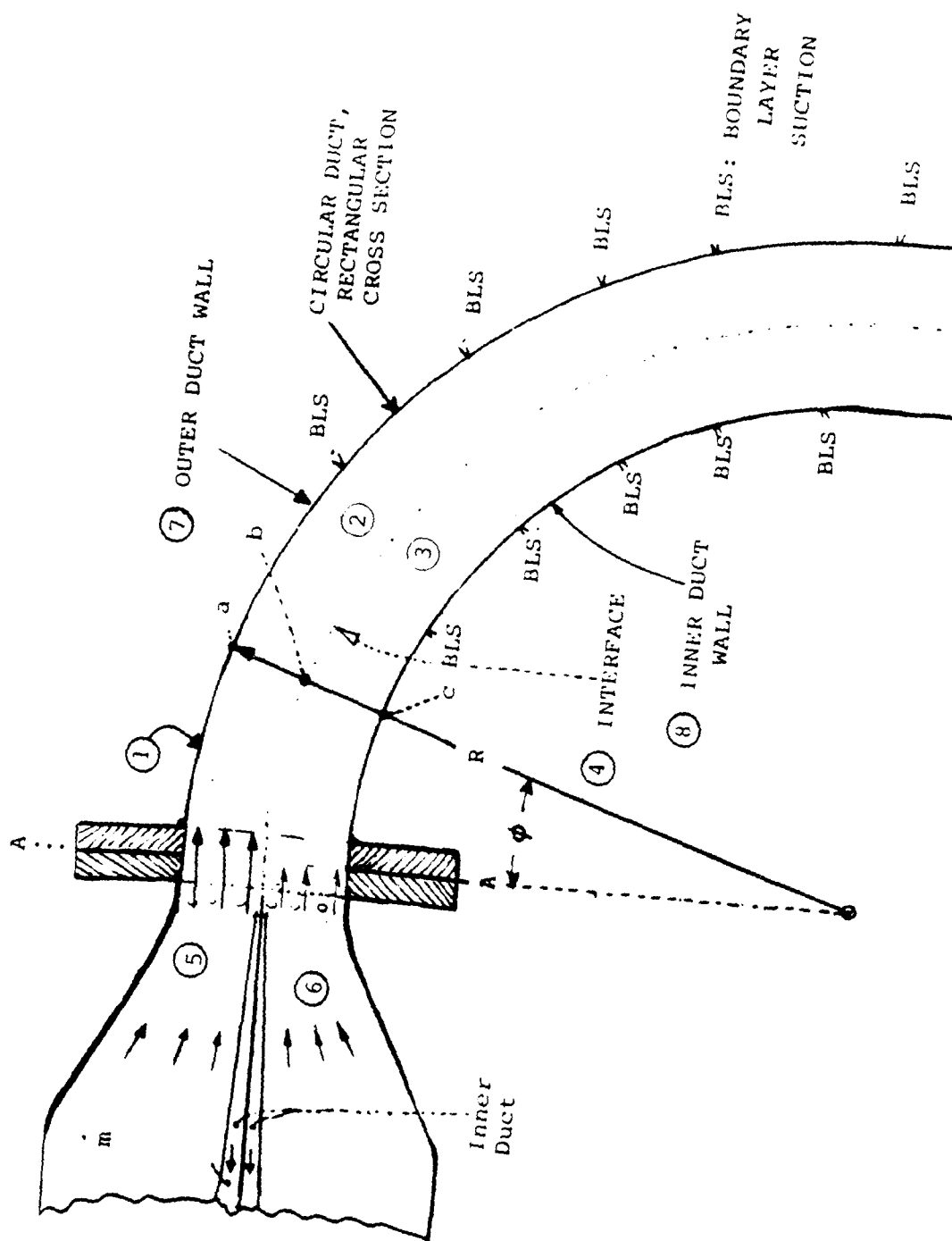


Figure 2. Schematic of the Curved Flow Channel. Directions will be made at seven stations spaced at  $\phi = 15^\circ$  in the Radial and Spanwise

A general discussion of the effects of streamline curvature on turbulent flow is given by Bradshaw in Reference 2. He points out that there is a "surprising large effect" of streamline curvature on shear-flow turbulence. Bradshaw<sup>2</sup> further states that ". . . many flows of aeronautical or engineering interest will be significantly affected, or even dominated, by the direct effect of streamline curvature on the turbulence." Thus, we believe that the study proposed will not only be useful for better understanding of flow in a Radiax turbine but will provide information of a fundamental nature that would be useful in many engineering applications.

According to Bradshaw<sup>2</sup> in his history of research of curved turbulent flows, early experimental work was done by Wendt<sup>4</sup>, Wattendorf<sup>5</sup>, and Schmedbauer<sup>6</sup>. It started with investigations in 1928 by Wattendorf and MacColl<sup>7</sup> of boundary layer flow in a curved channel of constant curvature. This research was carried further by Wilcken<sup>3</sup> in 1930. Wendt<sup>4</sup> in 1933 measured turbulent flow between two coaxial cylinders. This was followed by Schmedbauer<sup>6</sup> in 1936 who studied more deeply the turbulent boundary layer flow on convex surfaces.

Meanwhile Wattendorf, who by then had joined von Karman at the California Institute of Technology, investigated fully developed turbulent flow in curved channels, as compared with the earlier boundary layer work. He then extended these studies to the flow between concentric rotating cylinders of the same curvature, in order to obtain direct comparison between rotation and curvature. A new dimension was added in 1933 when Wattendorf and Kuethe developed a hot wire apparatus for direct measurements of the correlation between root mean square velocity fluctuations and turbulent friction<sup>8</sup>.

Little attention was paid to curved flow for about the next 20 years, when Eskanazi and Yeh<sup>9</sup> of Johns Hopkins University, in 1956, duplicated the earlier Wattendorf

experiments at the California Institute of Technology, in order to establish a base. They then carried the research further, also using the hot wire anemometer for the direct measurement of momentum exchange.

According to Bradshaw<sup>2</sup> the first study of wall jets on plane surfaces was done by Forthmann<sup>10</sup> in 1934. However, research on a wall jet in contact with a curved boundary, again according to Bradshaw<sup>2</sup>, did not occur until the 1960's by Newman<sup>11</sup> and Bradshaw and Gee<sup>12</sup>. In discussing a paper by Stratford, Jawor, and Smith<sup>13</sup>, Bradshaw<sup>2</sup> states, "They discuss mechanisms by which curvature could affect spreading rate even if the two streams had the same total pressure (but different density and velocity) but the arguments are not conclusive and even today there is no data of such flows."

More recently (1982) El-Taher<sup>14</sup> has investigated a ventilated wall jet on a straight wall. Figure 3 shows a schematic profile of the ventilated wall jet taken from Reference 14. Still more recently (November 1983) El-Taher<sup>15</sup> has investigated the ventilated wall jet as a circular arc. A schematic of the concept is shown on Figure 4 which was taken from Reference 15. El-Taher discusses recent experimental work in the study of wall jets. The work was limited to simple wall jets over circular cylinders or logarithmic spiral surfaces. Although these recent papers have data that are valuable to aid in understanding the proposed research, they are not duplicated in our current study.

In the studies just discussed, there was no boundary above or on the sides of the jets. Wood and Bradshaw<sup>16</sup>, in a 1982 paper, present experimental results for a jet along a flat surface that is constrained by solid surfaces. A schematic of their test rig is shown in Figure 5.

It is interesting to note that no research is reported on the more general case of curved channel flows with

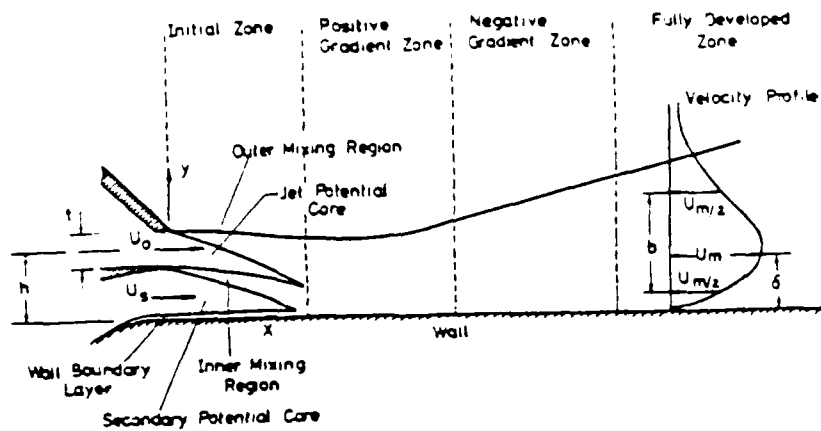


Figure 3. Schematic Profile of Ventilated Wall Jet (from Reference 14).

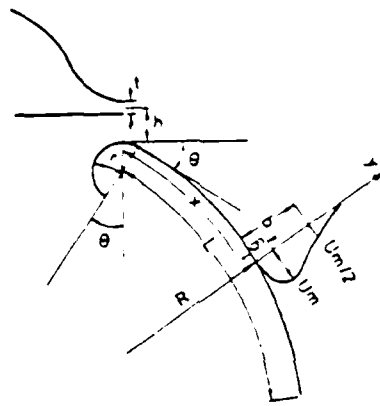


Figure 4. Schematic Profile of a Ventilated Jet of a Circular Arc (from Reference 15).

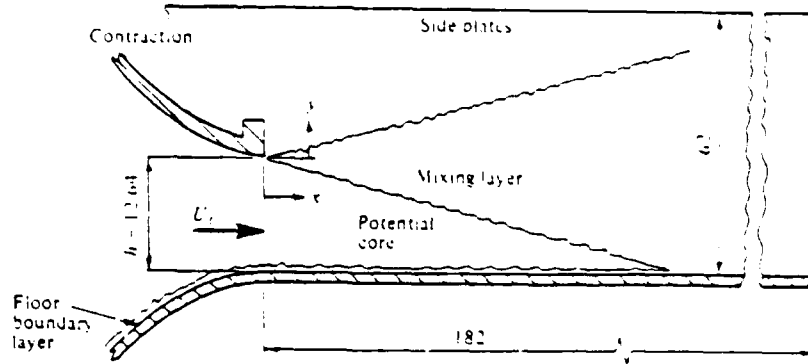


Figure 5. Schematic Diagram of Test Rig from Reference 16.  
All Dimensions in Centimeters.

two adjacent streams of different aeromechanical conditions. The reported interface phenomena of "wall jets" or "ventilated wall jets" may be vastly different from those expected in our planned research. For example, conditions can be varied from stable where the flow along the convex wall surface has a smaller total pressure than the flow along the concave wall surface, to unstable where the flow along the convex surface has the greater total pressure.

Wang in Reference 17 presents studies closely related to the work that we are doing. In his study Helium and air were used in a curved channel giving a density ratio of 7 to 1. Our experiments will use different refrigerants and will therefore cover a wider variation in density ratios. In addition heated air will be used in conjunction with cold air which will enable us to study density ratio like 1.2 to 1. In addition the ratio of channel width to radius of curvature (the distance  $ac$  over  $R$  in Figure 2) is larger in our experiments than those used in Reference 17. Thus, our work does not duplicate the work of Reference 17 but adds important information needed to understand the complex flows that can be developed in curved channels with two flows of different densities.

#### 2.1.2 Discussion of Experimental Approach

The goal of the current research is to achieve a better understanding of the phenomena at the interface between two gas streams flowing through a two-dimensional channel of fairly high curvature. These two co-flowing gas streams (see Figure 2) may have different temperatures and velocities and may be of different physical nature. The main research efforts will focus on the physical conditions which govern the stability or instability of the interface between these two gas streams, the phenomena of entrainment and mixing at the shear layer, and the conditions under which large-scale vortices may occur.

Figure 2 represents a simple configuration that is well suited for studying the basic scientific principles concerning interface stability in a curved flow between two different gas streams.

Three types of instability mechanisms may occur in the general case of curved flow. The most general is Kelvin-Helmholtz instability which results for a velocity difference between the two streams. This form of instability will be present in almost all situations. Kelvin-Helmholtz instability exists if

$$U_o \neq U_i$$

The second form of instability is the Taylor-Görtler instability which is related to the centripetal and Coriolis forces. Taylor-Görtler instability exists if

$$\rho_i U_i^2 > \rho_o U_o^2$$

The third form of instability is the Rayleigh-Taylor instability which is related to the body forces being opposed to the density gradient. Rayleigh-Taylor instability exists in a curved flow if

$$\rho_i > \rho_o$$

Frequently in situations where one or more of these instabilities is present the form of the instability is replenished in the flow direction. For example, in the boundary layer on the outer wall of a curved channel the flow has a lower value of total pressure than the main flow and, therefore, has Taylor-Görtler instability. The well known streamwise vortical structures (Taylor-Görtler vortices) are set up by the instability and they bring the high energy flow to the wall where

it in turn slows down causing the instability to persist in the flow direction.

Rayleigh-Taylor instability in a curved channel can be continuously replenished by heating the outer wall and/or cooling the inner wall while a single gas flows in the channel. Experiments<sup>18,19</sup> in a straight channel in a gravitational field heated below and cooled above show roll cells (Benard cells) with orientation depending on the shape of the container.

In our experiments the instabilities are not replenished and, therefore, different structures would be likely.

In order to get a better understanding of the stability at an interface let us look more closely at the interface between two swirling flows of different density and velocity. The flow parameters of the outer swirl are indicated by sub "o", of the inner swirl by sub "i". In Figure 6 four significant cases are illustrated: stable, semi-stable, semi-unstable, and unstable. Each of these cases is discussed below.

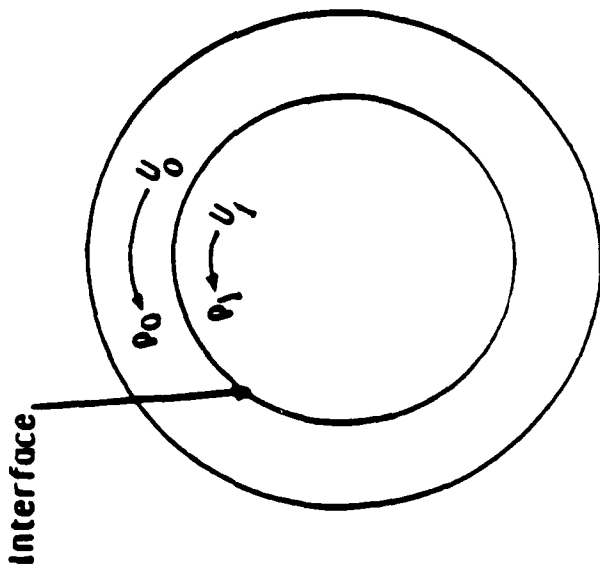
Case 1:  $\rho_i < \rho_o$  and  $\rho_i U_i^2 < \rho_o U_o^2$

Under these conditions, the interface is initially stable from a Taylor-Görtler and Rayleigh-Taylor perspective) and remains stable throughout any interaction. A distinction, however, due to Kelvin-Helmholtz instability can still be made between the following conditions:

$U_o = U_i$  This is a most stable condition (it corresponds to an inversion layer in meteorology).

$U_o < U_i$  Wave perturbations may exist at the interface, and momentum transfer from the inner to the outer swirl will occur.

## STABILITY REGIMES



Stable:	$\rho_1 \leq \rho_0$	;	$\rho_1 u_1^2 < \rho_0 u_0^2$
Semi Stable :	$\rho_1 > \rho_0$	;	$\rho_1 u_1^2 < \rho_0 u_0^2$
Semi Unstable :	$\rho_1 < \rho_0$	;	$\rho_1 u_1^2 > \rho_0 u_0^2$
Unstable:	$\rho_1 \geq \rho_0$	;	$\rho_1 u_1^2 > \rho_0 u_0^2$

Figure 6. Stability regimes for curved flows.

$U_o > U_i$       Wave perturbations may exist at the interface, and momentum transfer from the outer to the inner swirl will occur.

Thus, in a curved channel this type of flow would also be totally stable (except for the Kelvin-Helmholtz instability) and would be expected to produce the least activity at the interface.

Case 2:  $\rho_i > \rho_o$  and  $\rho_i U_i^2 < \rho_o U_o^2$

The two swirls are initially Taylor-Görtler stable at the interface. However, since  $U_o$  must be greater than  $U_i$  in order to satisfy the above given initial conditions, momentum is transferred from the low density outer flow to the high density inner flow which ultimately leads to the condition that  $\rho_i U_i^2 > \rho_o U_o^2$  which then becomes unstable. Therefore, Case 2 is called semi-stable. This happens because as studies of infrared suppression have shown that the transfer of momentum is much faster than the mixing process. The infrared suppression results suggest that even though momentum has been transferred from the outer stream to the inner stream the mixing is incomplete. Packets of gas exist that are still hot or cold, but have equal velocities with each other. It seems reasonable to assume that these packets are vortices that contain a major portion of one or the other of the gases. Mixing is not completed until these vortices have decayed. Thus, it takes much longer for the complete mixing to occur.

Due to the fact, that initially the two swirls are Taylor-Görtler stable the reorganization into the end condition requires a much longer time than those cases, where initially the two swirls are Taylor-Görtler unstable. However, as the cold flow is accelerated along the interface, a vigorous interaction can take place due to a transition to an unstable condition. The interface interaction will not be vigorous, however, if the size of the packets are small. The packets, just like particles, establish a drift velocity which depends on the density

difference (between the packet and the surroundings), the size of the packet, and the swirl velocity.

$$\text{Case 3: } \rho_i < \rho_o \text{ and } \rho_i U_i^2 > \rho_o U_o^2$$

The two swirl flows are initially Taylor-Görtler unstable, and therefore the interface disrupts immediately, and large eddies of high speed low density mass enter into the outer swirl of high mass density and lower speed. Velocity equilibration is quickly reached and the low density eddies are driven back toward the interface by buoyancy forces. This momentum exchange process is very intense, while irreversible mixing may be slight. We call this process momentum exchange under semi-unstable conditions of the interface.

$$\text{Case 4: } \rho_i > \rho_o \text{ and } \rho_i U_i^2 > \rho_o U_o^2$$

The two swirl flows are unstable. The inner swirl having both the larger density medium and the larger total pressure disrupts the interface and stays stably at the outside, while the outer medium having the lower density medium and the lower total pressure seeks the inner core and stays stably at the inside.

In the following an overview will be given of the potential influence on the interface phenomena of (a) the basic characteristics of the flow path configuration (geometry), and (b) the range of flow conditions (flow parameters).

#### 2.1.2.1 Characteristics of the Flow Path Configuration

In Figure 2 the two co-flowing gas streams of different temperature and velocity are indicated by (2) and (3); their interface is pictured by the dotted line (4). These two gas streams issue from the feed nozzles (5) and (6) at the inlet plane (A-A) to the curved flow channel (1).

For the experimental research the following provisions are made.

For minimizing three-dimensional flow effects in the curved flow channel, an aspect ratio of about 3.5:1 is chosen. Also, as shown in Figure 2, the use of boundary layer bleeding in the corners between the straight end walls and the curved channel walls (7) and (8) is provided.

For ensuring defined inlet conditions into the curved flow channel at plane (A-A), such as a low turbulence level and absence of wall boundary layers, a strong boundary layer bleed is provided along all the corners of the walls. Appropriate damping chambers for the hot and cold gas upstream of the inlet nozzles (5) and (6) are also provided as indicated in Figure 7 which gives an overall schematic view of the experimental rig.

#### 2.1.2.2 The Range of Flow Conditions

In the simplified geometry shown in Figure 2 we will only be interested in the interface phenomena and therefore have chosen to locate the interface, point b on the radius half way between the walls, points a and c along the radius (see Figure 2). This eliminates any consequences of the Coanda effect<sup>11</sup> that might occur for smaller values of the distance bc.

In view of the various types of stability that we discussed above we can set up a table of test conditions as shown in Table 1. Table 1 shows the combinations of total pressure for the inner ( $P_{0i}$ ) and outer ( $P_{0o}$ ) flow and the combinations of the static densities for the inner ( $\rho_i$ ) and outer ( $\rho_o$ ) flows. For each run type the larger values are indicated by the "greater than" sign (>) and an "equal" sign (=) indicates that the values are equal. Thus, for run type 5:

$$P_{0o} = P_{0i} \text{ and } \rho_o > \rho_i$$

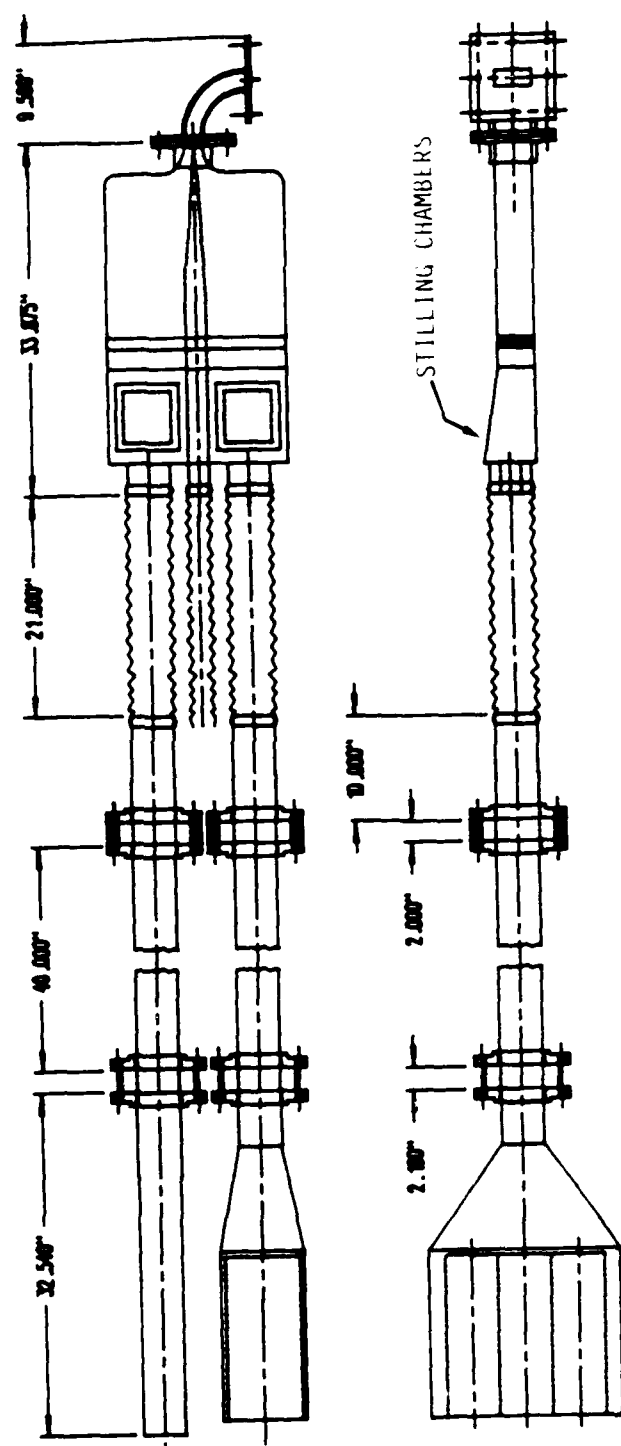


Figure 7. Schematic View of the Experimental Apparatus.

TABLE 1  
TEST COMBINATIONS OF TOTAL PRESSURE AND STATIC DENSITY

		Run Type							
		1	2	3	4	5	6	7	8
Inner Values	Outer Values	$p_o$	>	>			=	=	>
		$\rho_o$	>		>	>		=	
	$p_i$			>	>	=	=		>
		$\rho_i$		>		>		>	=

The first four run types are numbered in accordance with the stability discussion presented above and the stability is listed in Table 1.

Run types 5 through 8 are subsets of the first four but are listed separately because of the equality between one of the pairs of properties.

For given values of total pressure and total temperatures the values of velocity, mass flow rate and static density can be determined for expansion to local pressure in the test section. The ratios of total pressure and static density can be controlled and the total temperature ratio adjusted as required. Selected run types will be run at the same ratios but at different values of pressure thus allowing for different values of velocity or  $U^2/R$ .

We want to obtain the following types of data:

1. Static pressure measurements at the center of both the inner and outer wall.
2. Total pressure traverses spanwise at three locations along the radius at seven stations along the duct ( $\phi$  every 15° see Figure 2).
3. Total temperature traverses at the same stations.
4. Hot wire traverses at selected stations.
5. Flow visualization of the interface utilizing stroboscopic methods and high speed films.

Our main interests will be in the effects of the different stability criteria shown in Table 1 on the turbulent structure, the spreading of the mixing layer and their effects on any large coherent structures in the turbulent mixing layer that may be made visible by the flow visualization.

SECTION 3  
EXPERIMENTAL APPARATUS

In the first year of the contract the experimental apparatus was designed and fabricated. Figure 8 shows the layout of the apparatus with a list of numbers to identify the various components of the apparatus some of which will be used in the discussion that follows. The heavy gas is introduced into the apparatus through the inlet pipe marked 1 in Figure 8. This pipe is attached to a large, thin-walled, plastic bag that supplies the gas at one atmosphere. The bag is large enough to permit run times of about twenty seconds.

The 4 inch pipe marked 5 is 10 diameters long to insure that it is flowing full before the flow enters the venturi located at 7. The venturi is a "Low Loss" design manufactured by Crone Manufacturing, Inc. of Tulsa, Oklahoma.

The flow leaves the venturi and enters the flow stilling chamber, 11, by way of the flexible hose 10. The flexible hoses 10 and 20 can be interchanged at the connections to the stilling chamber to alternate the flows in the test chamber, 22.

Air enters the apparatus through the electric heaters located at 12. The flow rate is measure by the second "Low Loss" venturi located at 17. The air enters the stilling chamber 11 via the flexible hose 20. The air is quieted in the stilling chamber by its passage through about 2.5 inches of open cell foam having a porosity of ten.

The small flexible hose 21 is attached to the inlet of a small compressor and is used to suck the boundary layer from the tip of the splitter plate located in the stilling chamber.

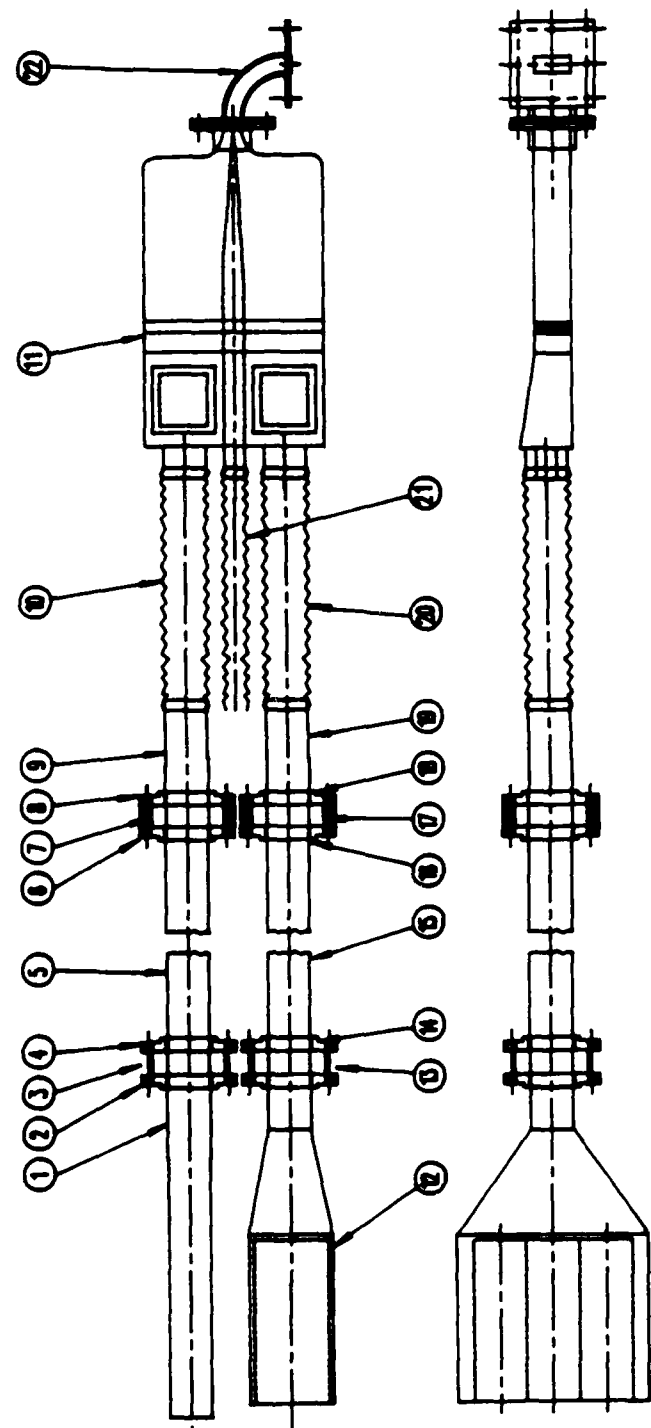


Figure 8. Experimental Apparatus Layout with the Various Elements Identified by Numbers.

Figure 9 shows a detail of the air heater which contains three 5.4 kw electric dryer elements. None, one, two or all three of the elements can be used for any given experiment. The maximum temperature that can be achieved with the heaters at maximum flow is 200°F.

Figure 10 shows the stilling chamber and splitter plate. As shown in Figure 11 the splitter plate extends slightly beyond the exit of the stilling chamber into the curved channel. The tip of the splitter plate is open and suction is applied to the tip via the small pipe located in the center at the back of the stilling chamber.

The flange at the exit of the stilling chamber is connected to the flange of the curved flow channel which is shown on Figure 10. The side walls of the chamber are made of specially fabricated curved plastic. The side plates are shown in an end view in Figure 12. A groove is cut into the top and bottom of each plate to provide for boundary layer suction in all four corners of the curved flow channel.

As shown in Figure 13 a transition section is attached to the exit of the curved flow channel and a flexible hose (not shown) connects the transition section to a compressor.

Although this feature was not used at this time, the flexible hoses at the inlet and exit wall permit the stilling chamber and the curved flow channel to be rotated as shown in Figure 14. The pivot point would be located at the center of the radius of curvature of the curved channel. In this way a stationary LVD system could be used to probe the curved flow channel, which has glass end plates (see Figure 12), at various stations.

High speed movies will also be made of the interface for various types of flow stability as discussed earlier.

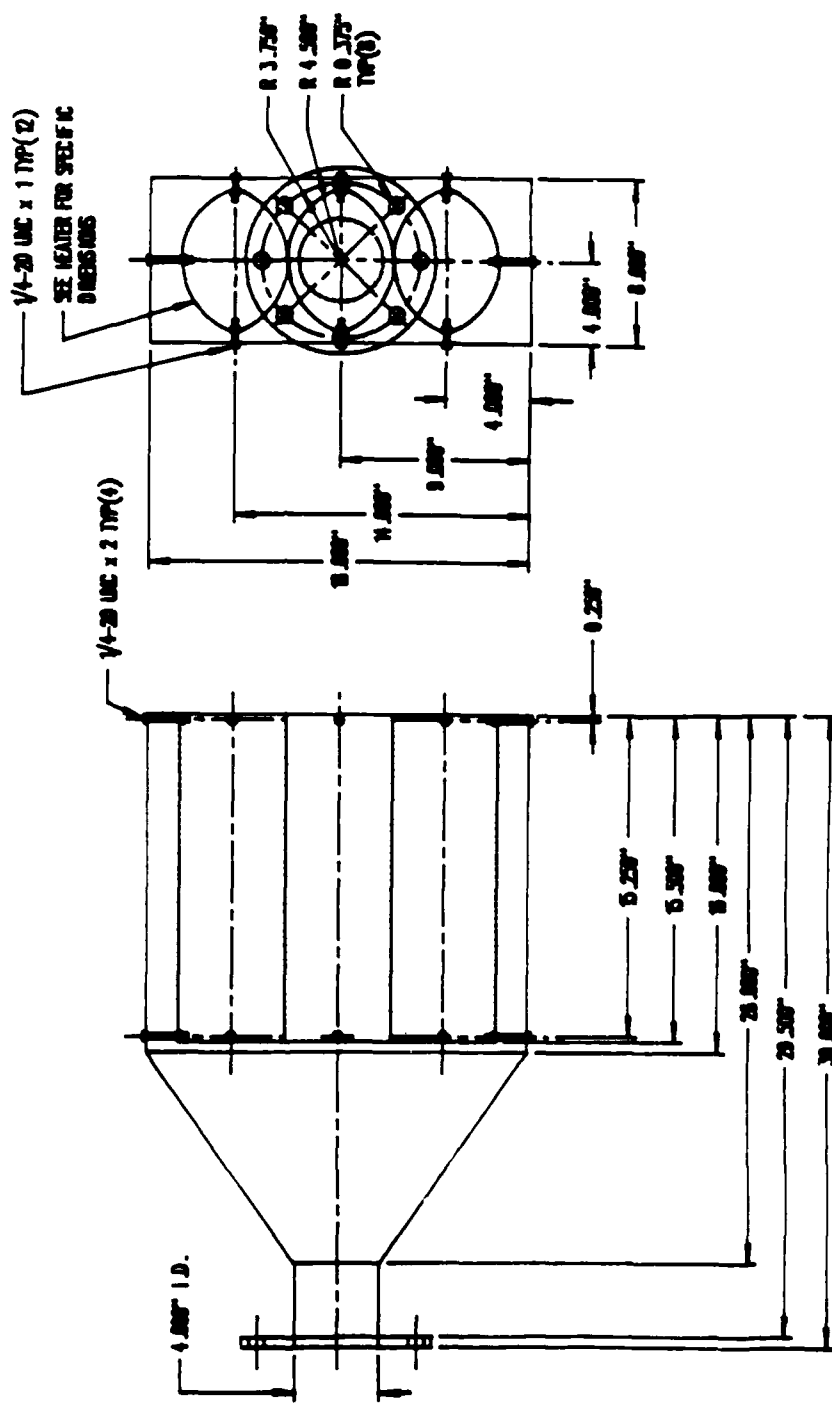


Figure 9. Electric Heaters Used to Heat the Incoming Air.

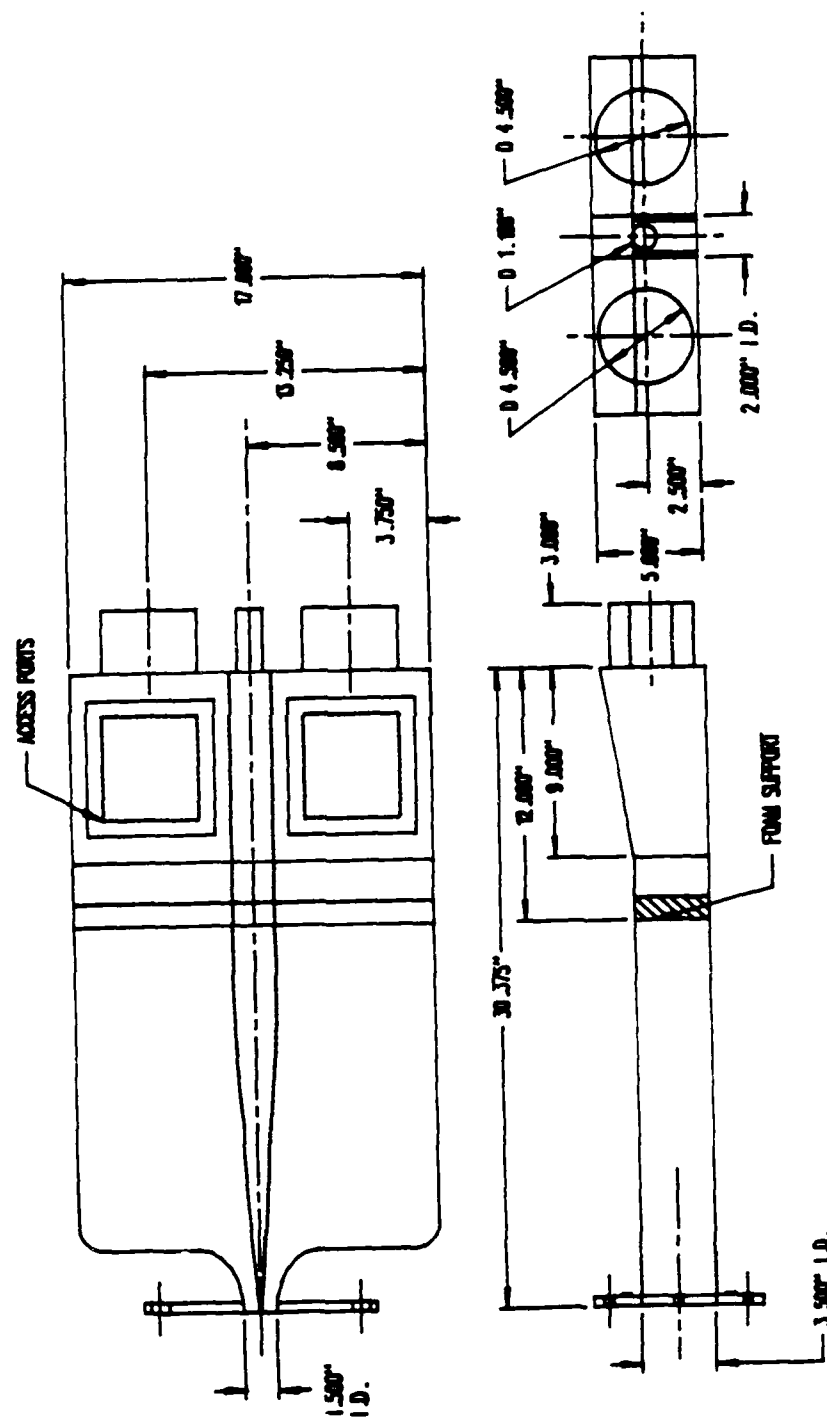


Figure 10. Stilling Chamber and Splitter Plate.

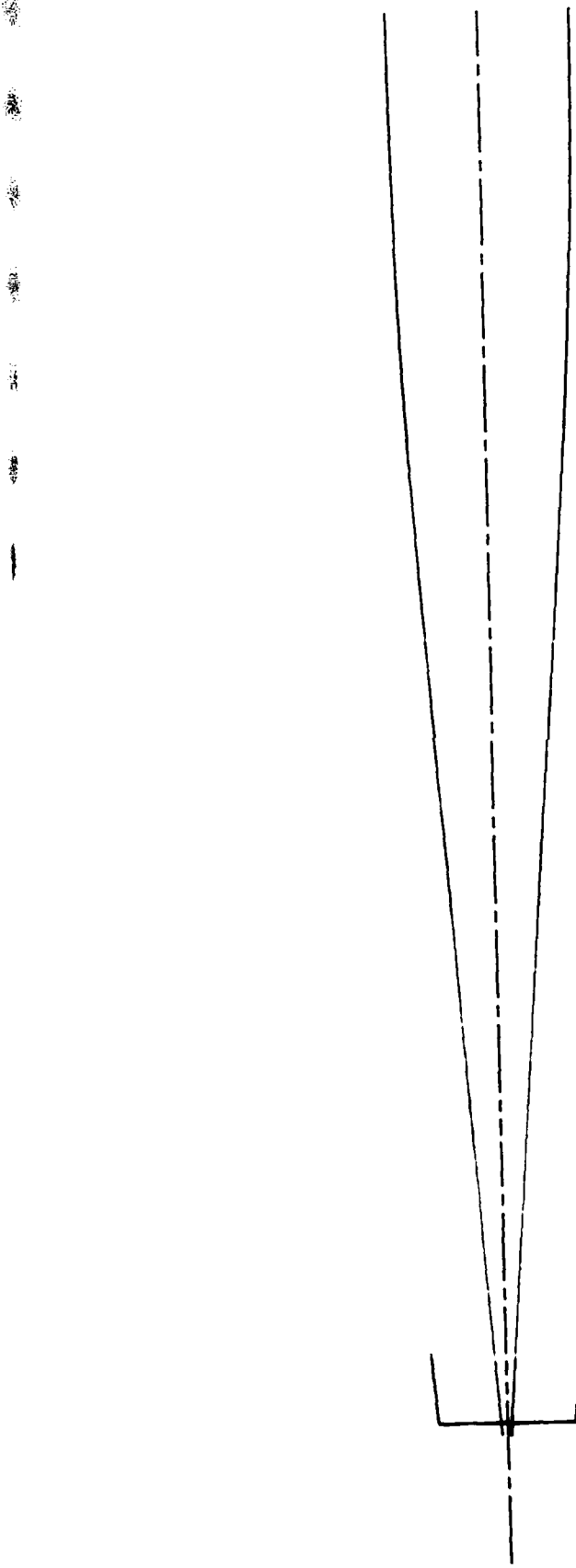


Figure 11. The Hollow Splitter Plate Extends Beyond the Exit of the Stilling Chamber.

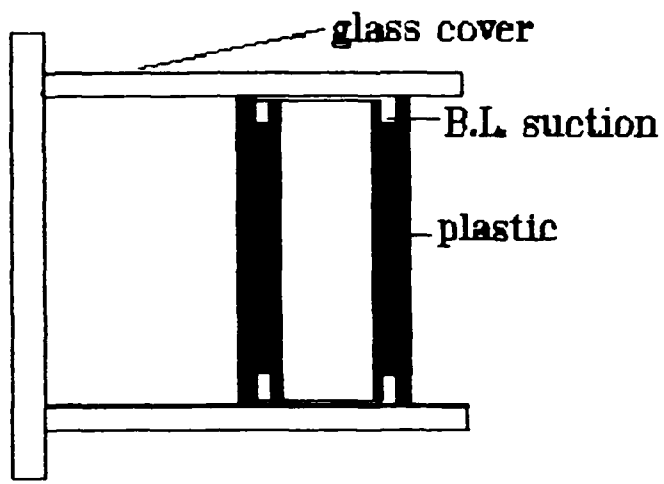


Figure 12. End View of Clear Plastic Side Plates Showing the Boundary Layer Suction Groves.

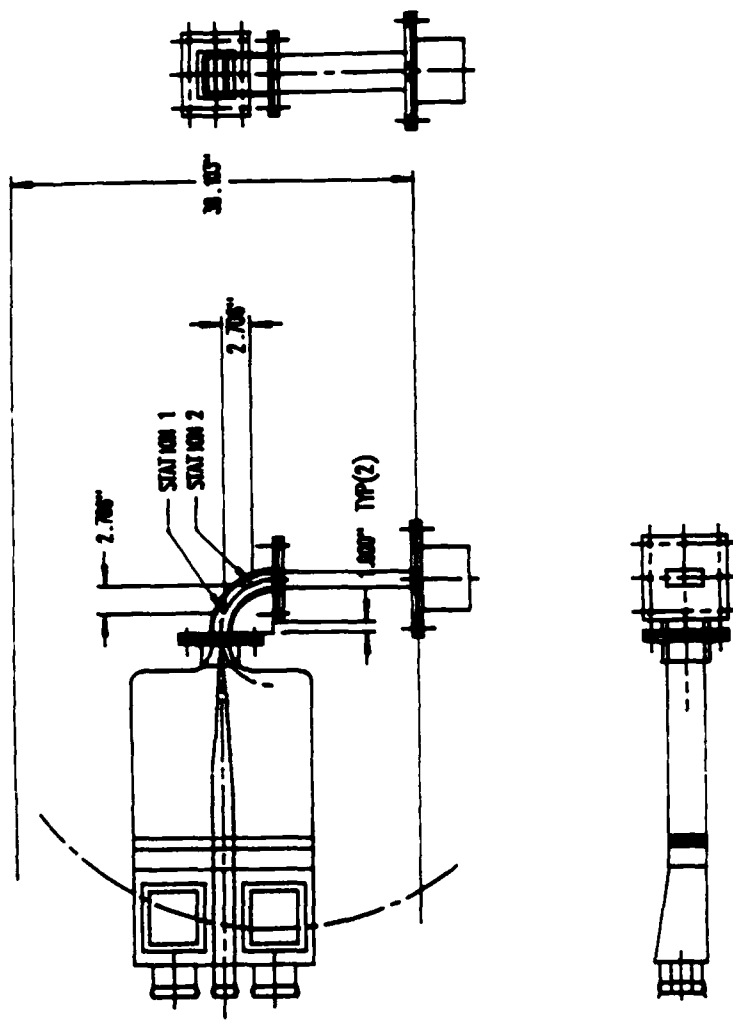


Figure 13. Transition Section Attached to the Curved Flow Channel.

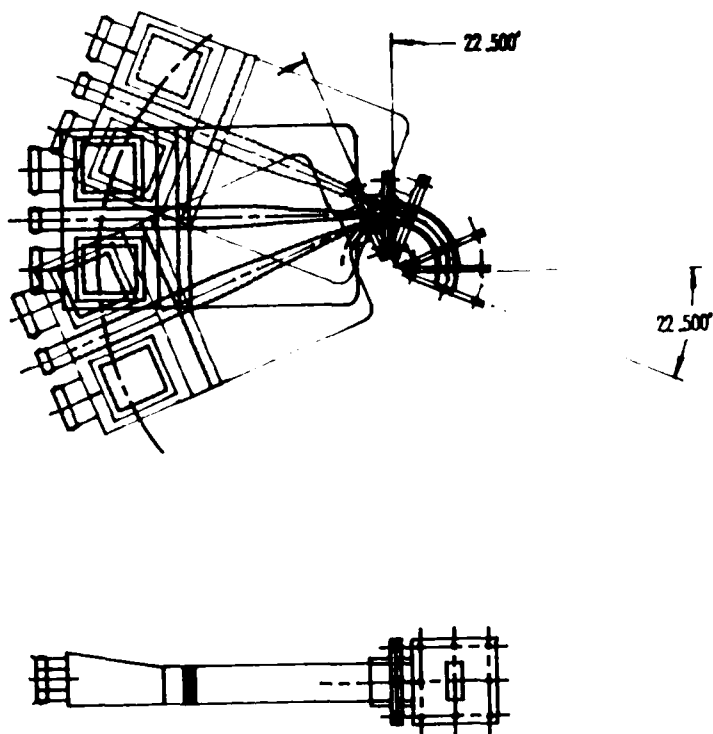


Figure 14. A Mount Could be Provided to Allow the Stilling Chamber and the Curved Channel to Pivot About the Center of the Channel.

All of the measured pressures and temperatures will be sampled by a MetraByte Dash-8, eight channel A/D converter board installed in a Zenith 160 portable computer with an internal 20 MB hard disk drive. Two MetraByte Exp-16 expansion sub-multiplexer boards will be connected to the Dash-8 to provide the capability of handling up to 30 channels of input data. Data sampling, storage, and display will be controlled by a compiled basic program.

## SECTION 4

### RESULTS

At this time the flow visualization aspects of the research have been nearly completed. A theatrical Meteor - Mr. Mista Fog Machine was used to generate a dense fog that was introduced into the flow channel at a number of different locations. The Mr. Mista Fog Machine was tested at Wright-Patterson Air Force Base by Dr. R. B. Rivir in his laboratory to determine the particle size using the liquid supplied by the manufacture for use with the fog machine. The preponderance of the droplets were below 5  $\mu\text{m}$  in size. The arithmetic mean was 2.2  $\mu\text{m}$ , the area mean 2.7  $\mu\text{m}$ , the volume mean 3.3  $\mu\text{m}$  and the Sauter mean was 5.0  $\mu\text{m}$ . Thus, the droplets are well suited for flow visualization and will closely follow the flow.

Four methods were used to photograph the flow.

- Black and white stills (35 mm) using a standard flash (3-4 milliseconds duration).
- High speed movies at speeds up to 8000 frames per second taken with a Photek camera.
- Standard VCR camera.
- Black and white stills (35 mm) using a high speed flash (3-4 microseconds).

The standard VCR photos are in real time and show the phenomena as it is seen in the lab. The black and white stills at the standard flash rate were not fast enough to show the structure in the flow, but did provide information on the overall flow. The high speed movies provided very informative flow visualization, but the best pictures of the structure were obtained from the high speed flash photographs.

A number of segments from the high speed films were put together on a TV tape that shows a number of different stability situations. A copy of the tape was supplied to AFOSR under separate cover.

An example photograph of each of the types of stability shown on Table 1 is presented in Figures 15 through 20; each shows the air temperature ( $^{\circ}\text{C}$ ), velocity (m/s) and dynamic pressure (Pa). The radius of curvature of the centerline of the channel is 0.127 m (5 inches). To enable easier comparison among figures we have grouped all of them together at the end of the section.

Photo Set 1 (Figures 15.A. and 15.B.) is a comparison of two gases (air) of the same density and temperature with different flow conditions which gives an indication of the Kelvin-Helmholtz and the Taylor-Görtler instability as described in Section 2.1.2. Since the densities are equal we can discern nothing about the Rayleigh-Taylor instabilities. The photos of the stable conditions, Set 1 a,c,e and g, (Run Type 7 from Table 1) represent flow conditions with higher velocity and total pressure on the outer curve. We can clearly see that the flow remains quite stable throughout the entire  $90^{\circ}$  curve with the smoke spreading to only four to eight times the thickness of the injected smoke. The photos of the unstable conditions, Set 1 b,d,f and h), (Run Type 8, Table 1) show that the flow quickly goes to the outer wall; in b,d and f it reaches the outer wall within  $30^{\circ}$ - $45^{\circ}$  of the plane of injection. The photos, in Set 2 represent conditions of neutral stability since the velocity, pressure and density inlet conditions are all equal. We can see that the spreading of the smoke is increased from the stable case, but less than in the unstable case with much less impinging on the outer wall. Most interaction with the wall occurs at or near  $90^{\circ}$  from the inlet at the bottom wall. This may be a result

of the wake behind the splitter plate which is moving slower than the main stream.

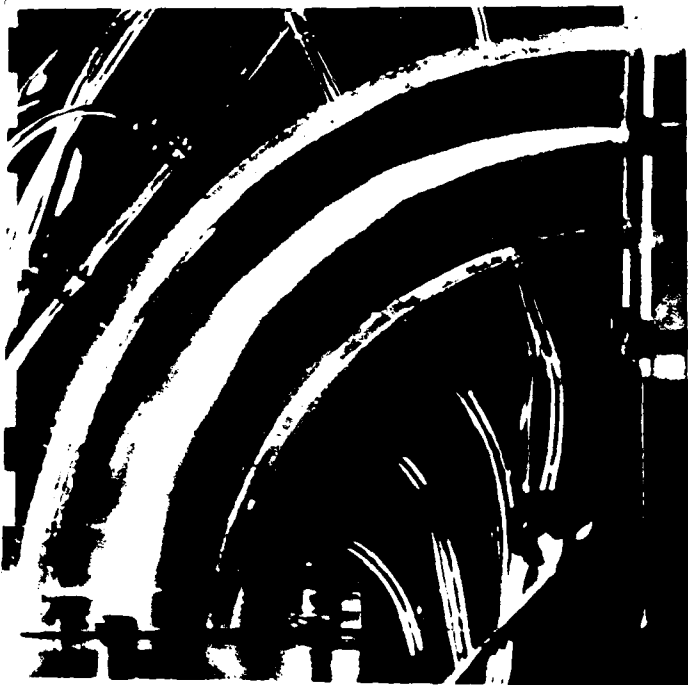
Photo Set 3 represents flow conditions similar to those in Set 1, but taken with a high speed flash. In these pictures we see similar flow conditions to what we saw in Set 1, but a much better resolution of actual structure within the flow. With these pictures we can see coherent structure within the mixing interface. These structures can be seen developing in the video tapes of the high speed movies and can be seen progressing through the entire test section. The thickness of the smoke is much less in these photographs than in Set 1. The slower flash speed integrates a flapping and pulsing of the smoke that can be seen in the high speed films. Thus, the actual location of the smoke varies with time and photographs at high speed capture it at an instantaneous location while the longer flash captures a range of locations. The TV tapes and high speed film show the flapping and confirms a total extent close to that seen in Set 1.

Photo Set 4 represents a comparison of the effects of density by means of heating either the inner or outer flowfield. A comparison of the mixing at two similar total pressures but different densities gives a qualitative effect of the densities. Consider Set 4 a and b, with dynamic pressure,  $q$ , on the outer curve of 4277 Pa and  $q$  on the inner curve of 356 Pa; the first with the outer flow heated (Set 4 a) and the second with the inner flow heated (Set 4 b). With the higher density on the outer flow (Run Type 1) the mixing is less than with the higher density on the inner flow (Run Type 2). The reverse seems to hold on Set 4 e and f while Set 4 c,d and g,h show little difference in mixing.

Photo Set 5 represents flows of equal total pressure but different velocities and densities. This gives a comparison of the Kelvin-Helmholtz and Rayleigh-Taylor instabilities. In Set 5 a,c,e and g are Run Type 6 and b,d,f and h are Run Type 5. Run

Type 6 is unstable in a Rayleigh-Taylor sense only after the slower inner flow is accelerated. However, there is very little difference that can be observed between Run Types 5 and 6 in Set 5.

Photo Set 6 represents flow of nearly equal velocity but different total pressure and density. This gives a comparison of the Taylor-Görtler and Rayleigh-Taylor instabilities.



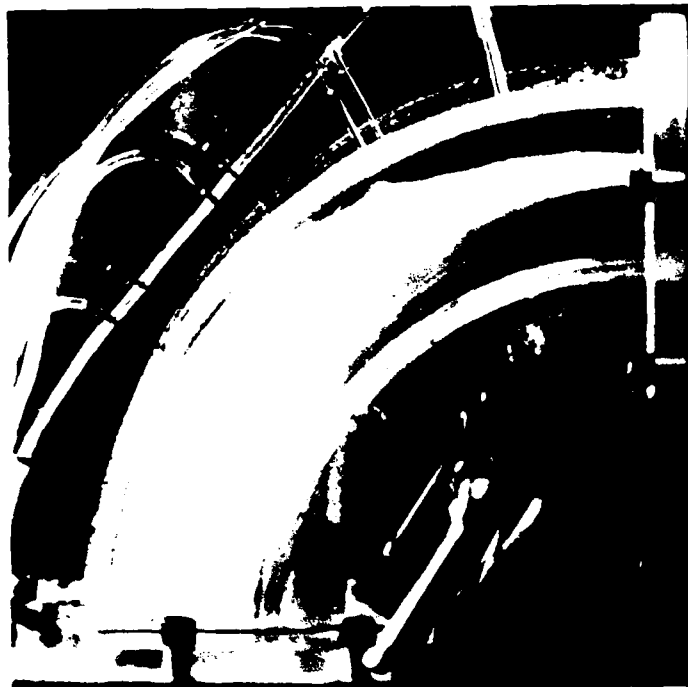
a) Top Air: 20°C 84.3 m/s 4277 Pa  
Bottom Air: 20°C 24.3 m/s 356 Pa



b) Top Air: 20°C 24.3 m/s 356 Pa  
Bottom Air: 20°C 84.3 m/s 4277 Pa



c) Top Air: 20°C 68.8 m/s 2851 Pa  
Bottom Air: 20°C 24.3 m/s 356 Pa



d) Top Air: 20°C 24.3 m/s 356 Pa  
Bottom Air: 20°C 68.8 m/s 2851 Pa

Figure 15.A. Air at equal densities, various velocities and dynamic pressures.  
Set 1 (a,b,c, and d).



e) Top Air: 20°C 48.6 m/s 1426 Pa  
Bottom Air: 20°C 24.3 m/s 356 Pa



f) Top Air: 20°C 24.3 m/s 356 Pa  
Bottom Air: 20°C 48.6 m/s 1426 Pa



g) Top Air: 20°C 34.4 m/s 713 Pa  
Bottom Air: 20°C 24.3 m/s 356 Pa



h) Top Air: 20°C 24.3 m/s 356 Pa  
Bottom Air: 20°C 34.4 m/s 713 Pa

Figure 15.B. Air at equal densities, various velocities and dynamic pressures.  
Set 1 (e,f,g, and h).



a) Top Air: 20°C 68.8 m/s 2851 Pa  
Bottom Air: 20°C 68.8 m/s 2851 Pa



b) Top Air: 20°C 48.6 m/s 1425 Pa  
Bottom Air: 20°C 48.6 m/s 1425 Pa

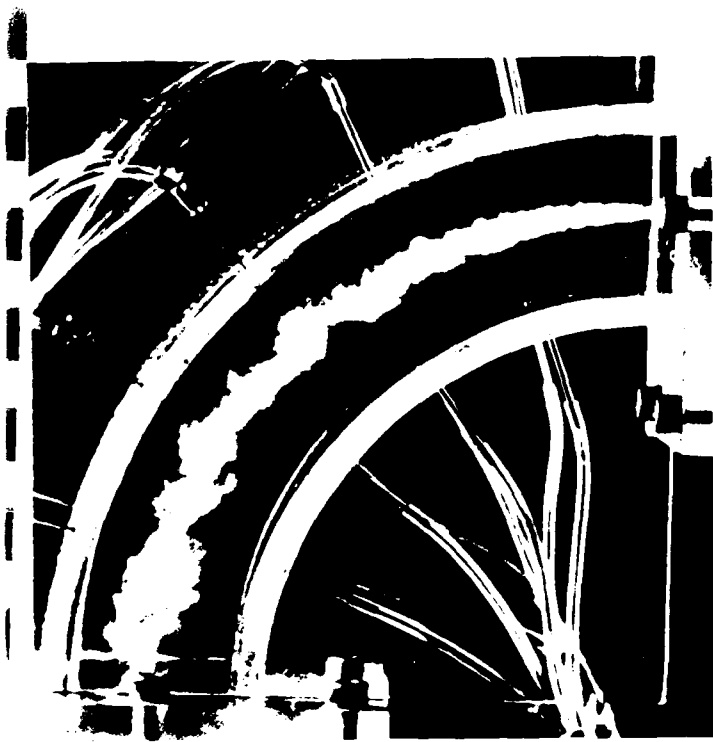


c) Top Air: 20°C 34.4 m/s 713 Pa  
Bottom Air: 20°C 34.4 m/s 713 Pa



d) Top Air: 20°C 24.3 m/s 356 Pa  
Bottom Air: 20°C 24.3 m/s 356 Pa

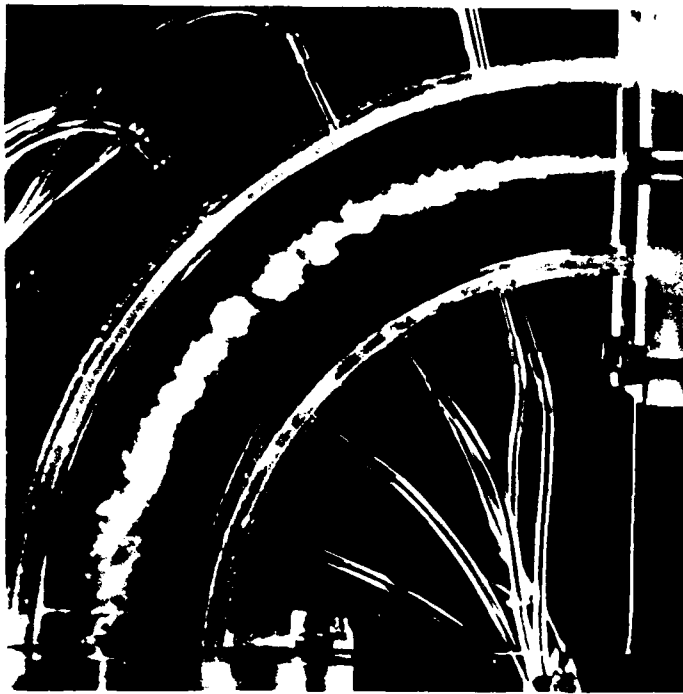
Figure 16.A. Air at equal densities and dynamic pressure with various velocities.  
Set 2 (a,b,c, and d).



a) Top Air: 20°C 84.3 m/s 4277 Pa  
Bottom Air: 20°C 24.3 m/s 356 Pa



b) Top Air: 20°C 24.3 m/s 356 Pa  
Bottom Air: 20°C 84.3 m/s 4277 Pa

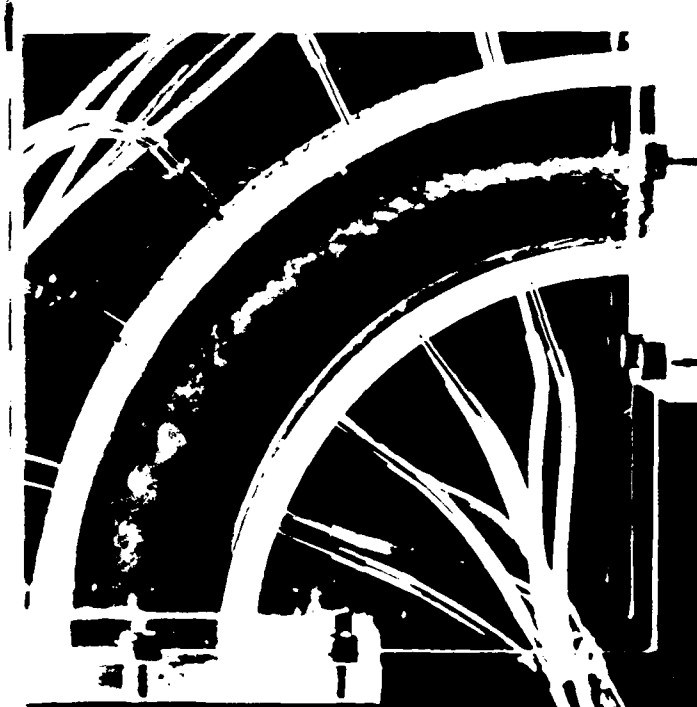


c) Top Air: 20°C 48.6 m/s 1426 Pa  
Bottom Air: 20°C 24.3 m/s 356 Pa



d) Top Air: 20°C 24.3 m/s 356 Pa  
Bottom Air: 20°C 48.6 m/s 1426 Pa

Figure 17.A. High speed flash of air-air at equal densities. Set 3 (a,b,c, and d). Compare Set 3 (a,b) to Set 1 (a,b); Set 3 (c,d) to Set 1 (e,f).



e) Top Air: 20°C 34.4 m/s 713 Pa  
Bottom Air: 20°C 24.3 m/s 356 Pa



f) Top Air: 20°C 24.3 m/s 356 Pa  
Bottom Air: 20°C 34.4 m/s 713 Pa



g) Top Air: 20°C 48.6 m/s 1426 Pa  
Bottom Air: 20°C 48.6 m/s 1426 Pa

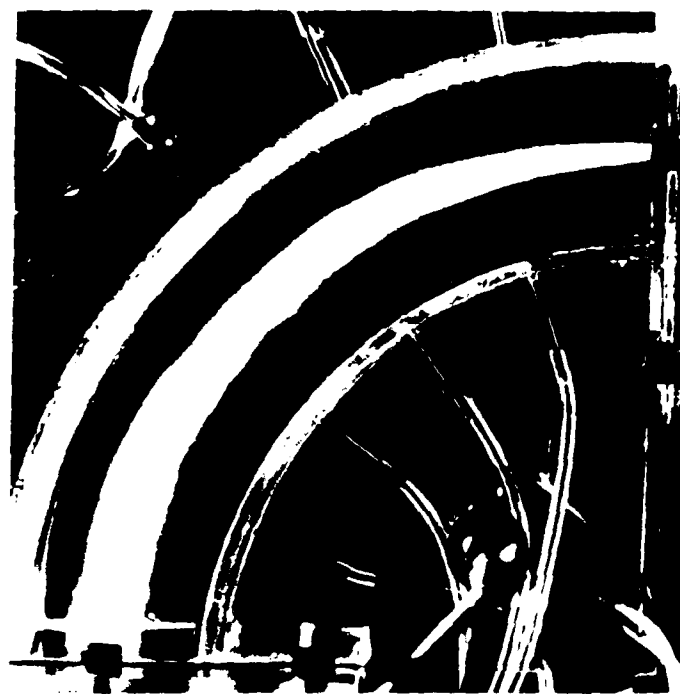
Figure 17.B. High speed flash of air-air at equal densities. Set 3 (e,f, and g).  
Compare Set 3 (e,f) to Set 1 (g,h) and Set 3 (g) to Set 2 (b).



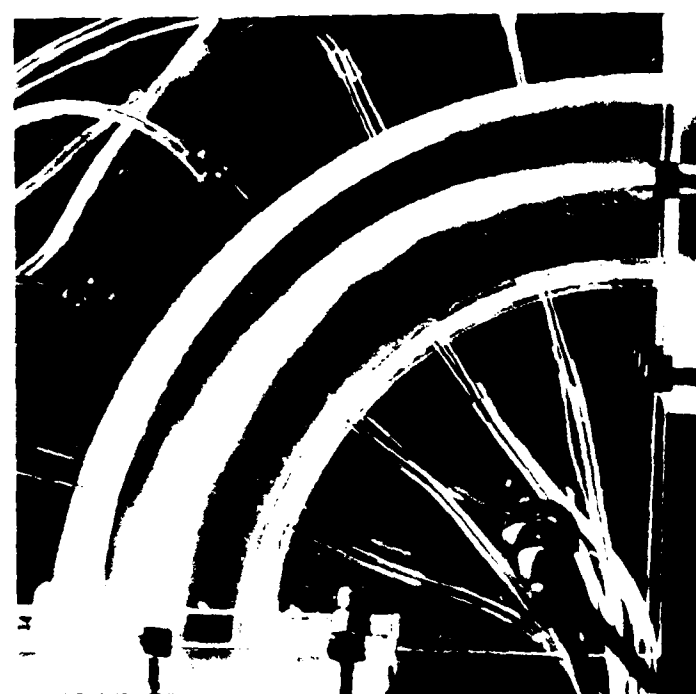
a) Top Heated Air:  $86^{\circ}\text{C}$   $93.3 \text{ m/s}$   
 $4277 \text{ Pa}$   
Bottom Air:  $20^{\circ}\text{C}$   $24.3 \text{ m/s}$   $356 \text{ Pa}$



b) Top Air:  $20^{\circ}\text{C}$   $84.3 \text{ m/s}$   $4277 \text{ Pa}$   
Bottom Heated Air:  $86^{\circ}\text{C}$   $26.9 \text{ m/s}$   
 $356 \text{ Pa}$



c) Top Heated Air:  $86^{\circ}\text{C}$   $76.2 \text{ m/s}$   
 $2851 \text{ Pa}$   
Bottom Air:  $20^{\circ}\text{C}$   $24.3 \text{ m/s}$   $356 \text{ Pa}$

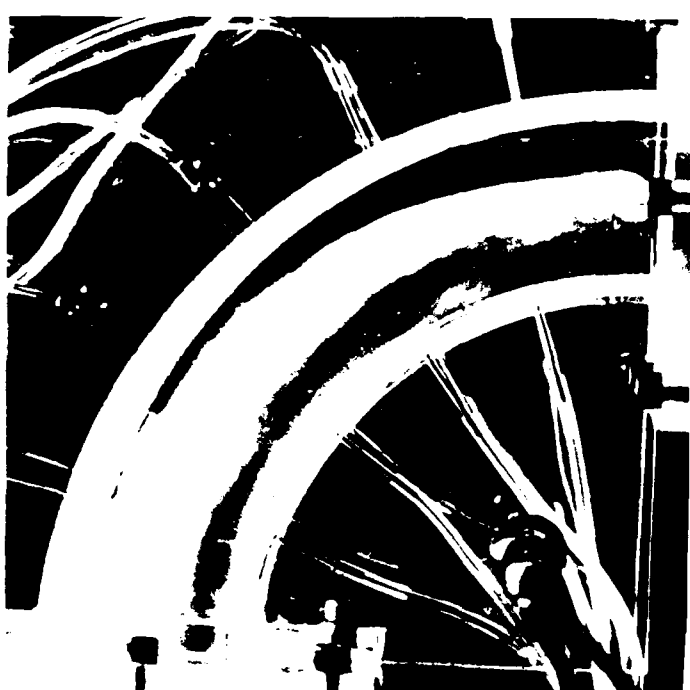


d) Top Air:  $20^{\circ}\text{C}$   $68.8 \text{ m/s}$   $2851 \text{ Pa}$   
Bottom Heated Air:  $86^{\circ}\text{C}$   $26.9 \text{ m/s}$   
 $356 \text{ Pa}$

Figure 18.A. Air at various densities, velocities, and dynamic pressures.  
Set 4 (a,b,c, and d).



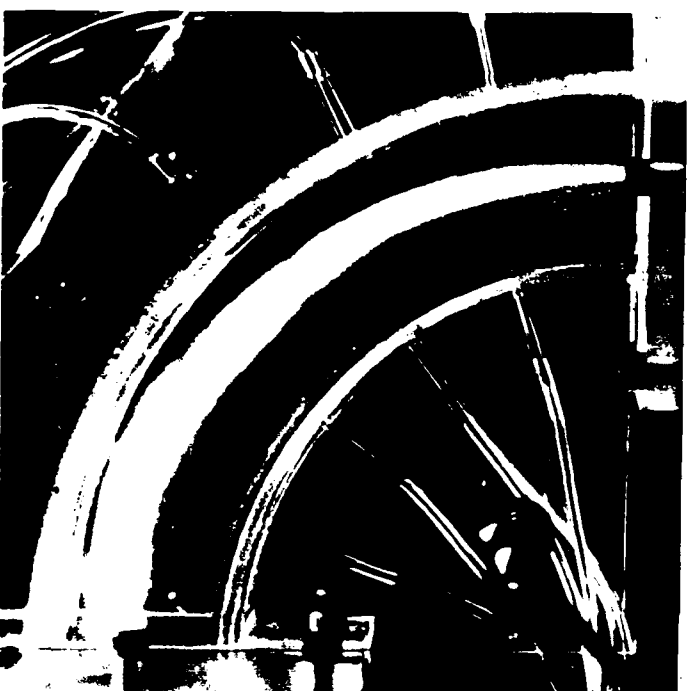
e) Top Heated Air:  $86^{\circ}\text{C}$  53.9 m/s  
1426 Pa  
Bottom Air:  $20^{\circ}\text{C}$  24.3 m/s 356 Pa



f) Top Air:  $20^{\circ}\text{C}$  48.6 m/s 1425 Pa  
Bottom Heated Air:  $86^{\circ}\text{C}$  26.9 m/s  
356 Pa

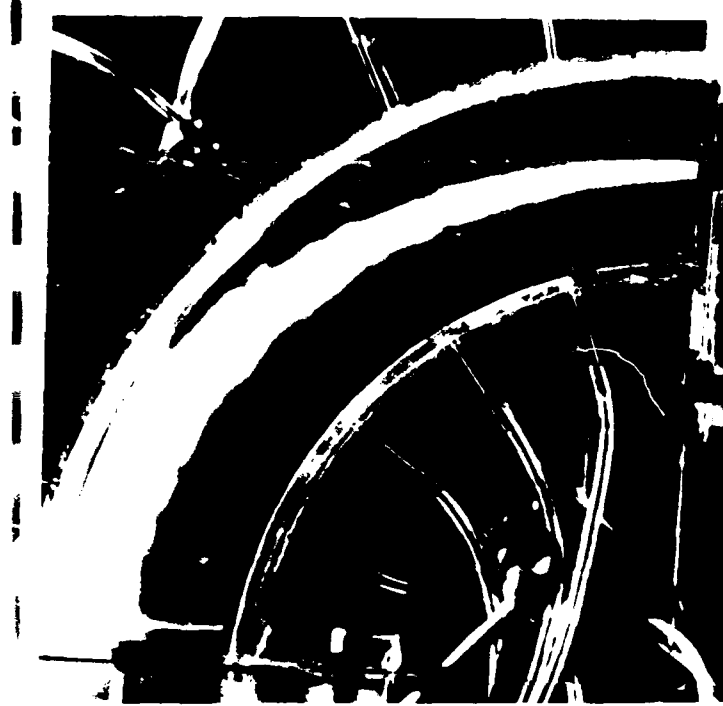


g) Top Heated Air:  $86^{\circ}\text{C}$  38.1 m/s  
713 Pa  
Bottom Air:  $20^{\circ}\text{C}$  24.3 m/s 356 Pa

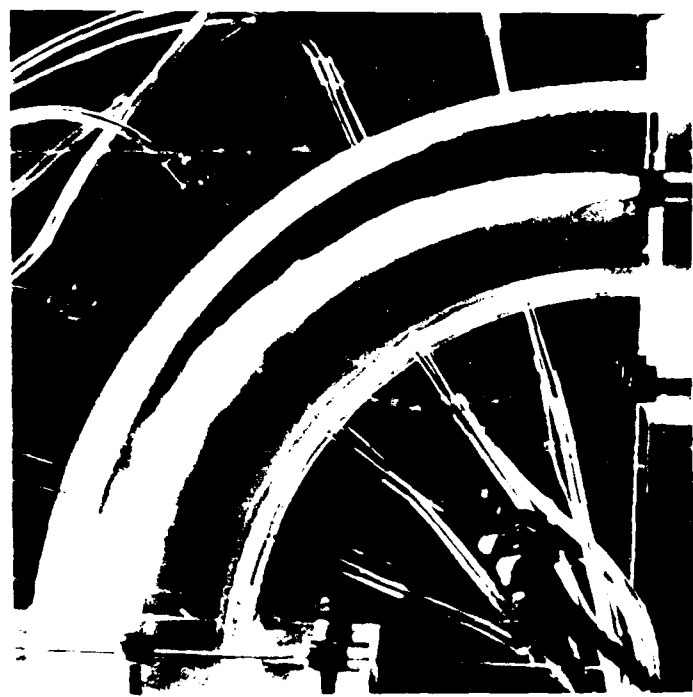


h) Top Air:  $20^{\circ}\text{C}$  34.4 m/s 713 Pa  
Bottom Heated Air:  $86^{\circ}\text{C}$  26.9 m/s  
356 Pa

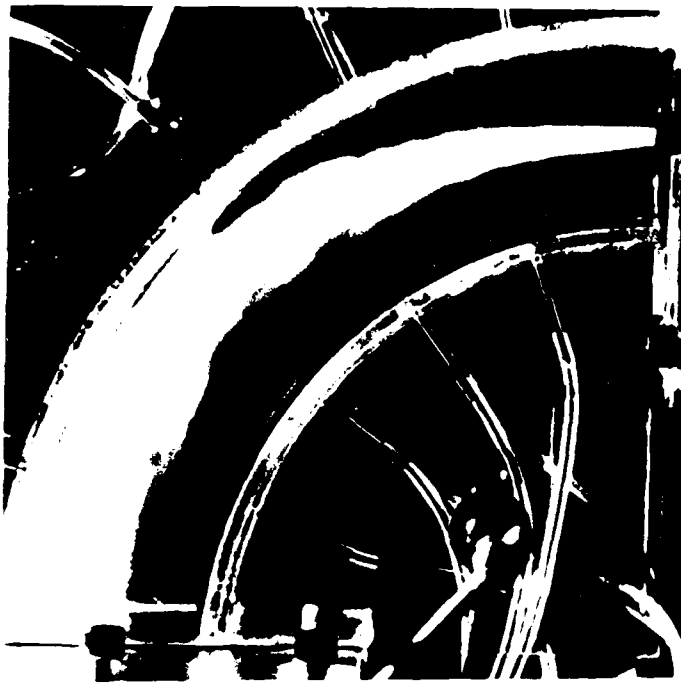
Figure 18.B. Air at various densities, velocities, and dynamic pressures.  
Set 4 (e, f, g, and h).



i) Top Heated Air:  $86^{\circ}\text{C}$  26.9 m/s  
356 Pa  
Bottom Air:  $20^{\circ}\text{C}$  34.4 m/s 713 Pa



j) Top Air:  $20^{\circ}\text{C}$  24.3 m/s 356 Pa  
Bottom Heated Air:  $86^{\circ}\text{C}$  38.1 m/s  
713 Pa



k) Top Heated Air:  $86^{\circ}\text{C}$  26.9 m/s  
356 Pa  
Bottom Air:  $20^{\circ}\text{C}$  48.6 m/s 1426 Pa



l) Top Air:  $20^{\circ}\text{C}$  24.3 m/s 356 Pa  
Bottom Heated Air:  $86^{\circ}\text{C}$  53.9 m/s  
1426 Pa

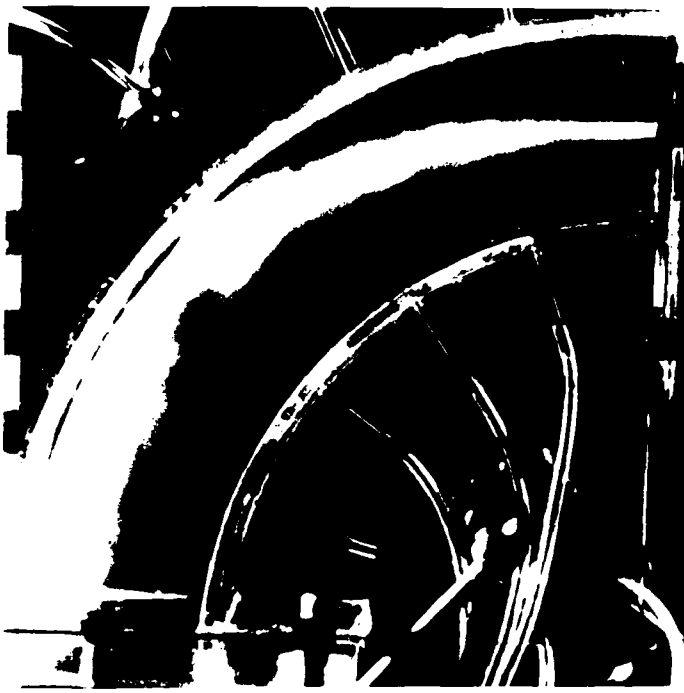
Figure 18.C. Air at various densities, velocities, and dynamic pressures.  
Set 4 (i,j,k, and l).



m) Top Heated Air: 86°C 26.9 m/s  
356 Pa  
Bottom Air: 20°C 68.8 m/s 2851 Pa



n) Top Air: 20°C 24.3 m/s 356 Pa  
Bottom Heated Air: 86°C 76.2 m/s  
2851 Pa



o) Top Heated Air: 86°C 26.9 m/s  
356 Pa  
Bottom Air: 20°C 84.3 m/s 4277 Pa

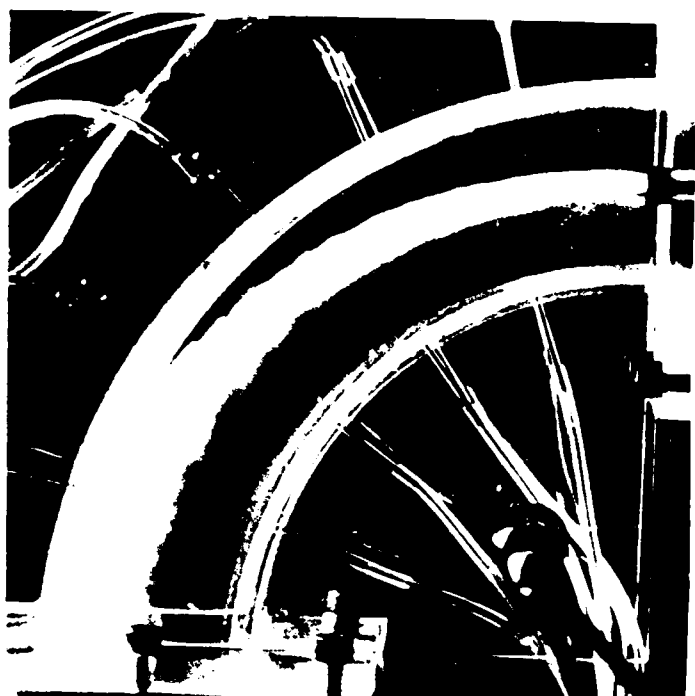


p) Top Air: 20°C 24.3 m/s 356 Pa  
Bottom Heated Air: 86°C 93.3 m/s  
4277 Pa

Figure 18.D. Air at various densities, velocities, and dynamic pressures.  
Set 4 (m,n,o, and p).



a) Top Heated Air:  $86^{\circ}\text{C}$   $26.9 \text{ m/s}$   
 $356 \text{ Pa}$   
Bottom Air:  $20^{\circ}\text{C}$   $24.3 \text{ m/s}$   $356 \text{ Pa}$



b) Top Air:  $20^{\circ}\text{C}$   $24.3 \text{ m/s}$   $356 \text{ Pa}$   
Bottom Heated Air:  $86^{\circ}\text{C}$   $26.9 \text{ m/s}$   
 $356 \text{ Pa}$



c) Top Heated Air:  $86^{\circ}\text{C}$   $38.1 \text{ m/s}$   
 $713 \text{ Pa}$   
Bottom Air:  $20^{\circ}\text{C}$   $34.4 \text{ m/s}$   $713 \text{ Pa}$



d) Top Air:  $20^{\circ}\text{C}$   $34.4 \text{ m/s}$   $713 \text{ Pa}$   
Bottom Heated Air:  $86^{\circ}\text{C}$   $38.1 \text{ m/s}$   
 $713 \text{ Pa}$

Figure 19.A. Air at equal dynamic pressures, various velocities and densities.  
Set 5 (a,b,c, and d).



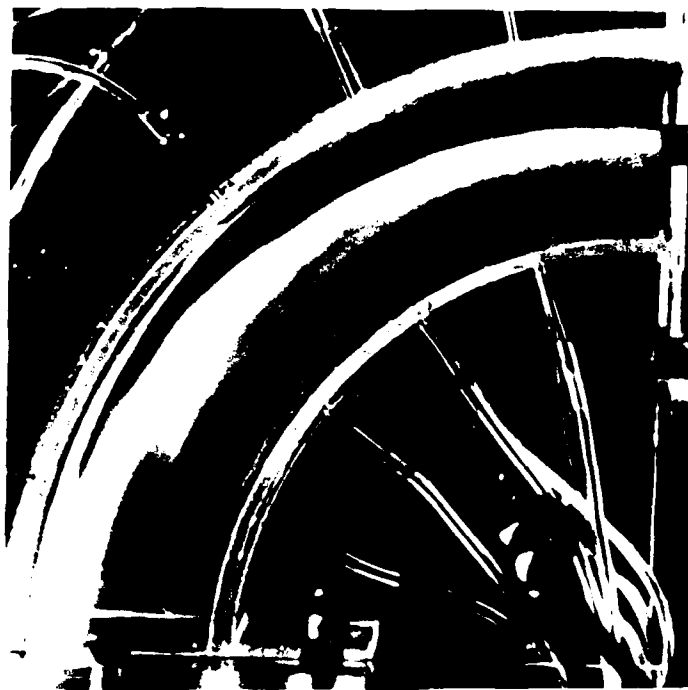
e) Top Heated Air:  $86^{\circ}\text{C}$   $53.9 \text{ m/s}$   
 $1426 \text{ Pa}$   
Bottom Air:  $20^{\circ}\text{C}$   $48.6 \text{ m/s}$   $1426 \text{ Pa}$



f) Top Air:  $20^{\circ}\text{C}$   $48.6 \text{ m/s}$   $1426 \text{ Pa}$   
Bottom Heated Air:  $86^{\circ}\text{C}$   $53.9 \text{ m/s}$   
 $1426 \text{ Pa}$



g) Top Heated Air:  $86^{\circ}\text{C}$   $76.2 \text{ m/s}$   
 $2851 \text{ Pa}$   
Bottom Air:  $20^{\circ}\text{C}$   $68.8 \text{ m/s}$   $2851 \text{ Pa}$



h) Top Air:  $20^{\circ}\text{C}$   $68.8 \text{ m/s}$   $2851 \text{ Pa}$   
Bottom Heated Air:  $86^{\circ}\text{C}$   $76.2 \text{ m/s}$   
 $2851 \text{ Pa}$

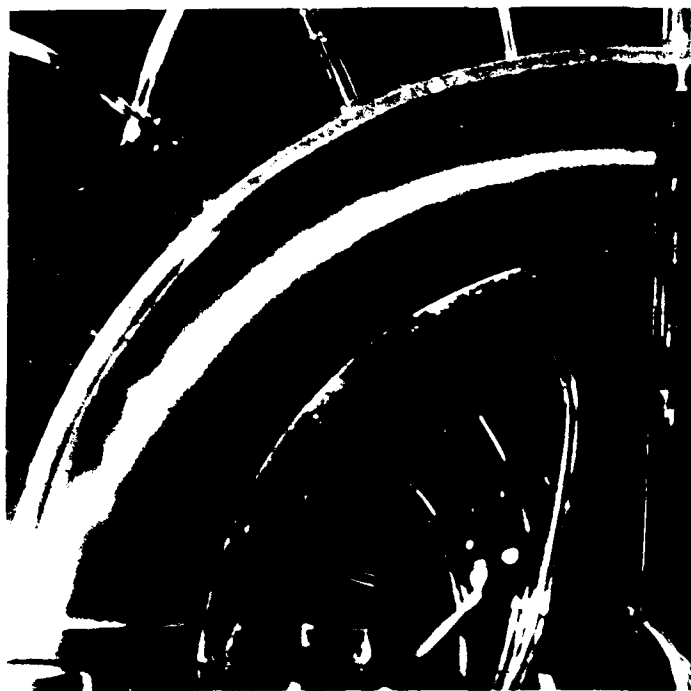
Figure 19.B. Air at equal dynamic pressures, various velocities and densities.  
Set 5 (e,f,g, and h).



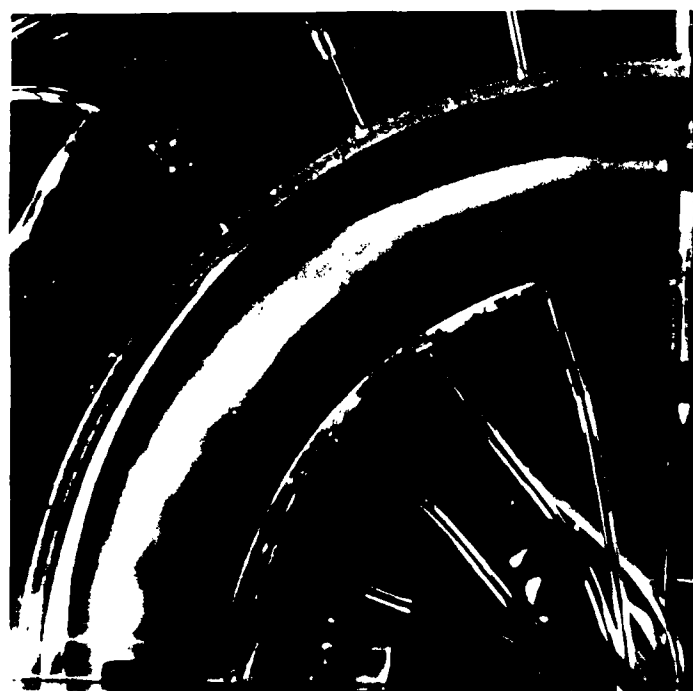
a) Top Heated Air:  $86^{\circ}\text{C}$   $38.1 \text{ m/s}$   
 $713 \text{ Pa}$   
Bottom Air:  $20^{\circ}\text{C}$   $38.5 \text{ m/s}$   $891 \text{ Pa}$



b) Top Air:  $20^{\circ}\text{C}$   $38.5 \text{ m/s}$   $891 \text{ Pa}$   
Bottom Heated Air:  $86^{\circ}\text{C}$   $38.1 \text{ m/s}$   
 $713 \text{ Pa}$

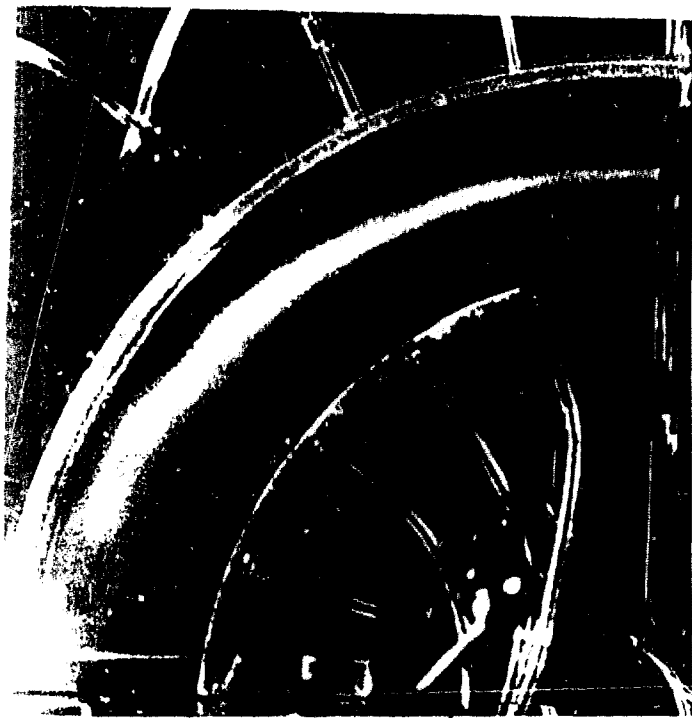


c) Top Heated Air:  $86^{\circ}\text{C}$   $53.9 \text{ m/s}$   
 $1426 \text{ Pa}$   
Bottom Air:  $20^{\circ}\text{C}$   $53.0 \text{ m/s}$   $1515 \text{ Pa}$



d) Top Air:  $20^{\circ}\text{C}$   $53.0 \text{ m/s}$   $1515 \text{ Pa}$   
Bottom Heated Air:  $86^{\circ}\text{C}$   $53.9 \text{ m/s}$   
 $1426 \text{ Pa}$

Figure 20.A. Air at equal velocities, various dynamic pressures and densities.  
Set 6 (a,b,c, and d).



e) Top Heated Air:  $86^{\circ}\text{C}$  76.2 m/s  
2851 Pa  
Bottom Air:  $20^{\circ}\text{C}$  76.9 m/s 3564 Pa



f) Top Air:  $20^{\circ}\text{C}$  76.9 m/s 3564 Pa  
Bottom Heated Air:  $86^{\circ}\text{C}$  76.2 m/s  
2851 Pa

Figure 20.B. Air at equal velocities, various dynamic pressures and densities.  
Set 6 (e,f).

## SECTION 5

### CONCLUSIONS

From the photographs presented the Kelvin-Helmholtz and Taylor-Görtler instabilities are the most significant forms of instability. The Rayleigh-Taylor instability plays a secondary role and is important only after an interaction occurs along the interface. If, as infrared information seems to suggest, coherent structures or packets of fluid are generated during the interaction which consists mainly of one or other (e.g. hot or cold) fluids, then concepts of semi-stable and semi-unstable follow from the density distribution. However, the magnitude of their instability depends on the size of the structures as well as the density difference, curvature, and velocity. The results we have obtained for the range of parameters tested indicate that the effect on stability is small over the 90° bend of the channel observed.

The Kelvin-Helmholtz instability causes a growth of the mixing region similar to that without curvature if the flow is Taylor-Görtler stable. However, at this time we have not determined the effect of the curvature on the spreading by comparing the results of a straight channel to those from the curved channel.

The Taylor-Görtler instability dominates the flow. If the flow is Taylor-Görtler unstable the smoke rapidly moves to the outer wall in the center of the channel. Near the side walls the high speed movies show that the smoke moves toward the inner wall. Thus, a three-dimensional flow is established in the channel and this type of flow appears to be inherently three-dimensional. Pitot tube and hot wire measurements will be made to determine more detail of the effects of the instability.

These results will be published in Capt. Michael Skomrock's thesis at a latter date.

These results will be published in Capt. Michael Skomrock's thesis at a later date.

When the flow is Taylor-Görtler stable as it is in the Radiax turbine cooling concept (see References 20 and 21) the two fluids flow separately through the curved channel and the flow remains primarily two-dimensional. Two-dimensional calculations using a full time-dependent, two-dimensional, Navier-Stokes code were reported for a Taylor-Görtler stable condition in Reference 20 for a curved channel. These calculations also indicated that the cooling flow would follow the curvature and cool the blade. Thus, the results shown in the photographs for the Taylor-Görtler stable situation demonstrate the essential flow features observed in the numerical simulation reported in Reference 20.

## SECTION 6

### RECOMMENDATIONS

The work will be continued to determine quantitative information using channel flow measurements from pitot tubes, thermocouples, and hot wires. Also, additional fast flash stills will be obtained for a wider range of parameters than are currently available and these results will be published in the open literature.

In addition, the following recommendations are made:

- Titanium tetrachloride should be used to identify the interact at the interface between the two streams.
- Very high speed flashes or lasers should be used to better determine the coherent structures that have been observed with the 3-4 ls flash.
- LDV measurements should be made of the flowfield using air and freon as well as air and heated air.
- Because of the inherent three-dimensional character of the flow, a full time-dependent, three-dimensional, Navier-Stokes computational simulation of the geometry for various conditions should be accomplished. We plan to look at a two-dimensional formulation in the current study to prepare for the three-dimensional calculations and gain insight into the Taylor-Görtler stable flows.
- High speed infrared photographs should be taken of air and heated-air to see if coherent structures of different temperatures can be indentified.

## SECTION 7

### REFERENCES

1. Bradshaw, P., "The Analogy Between Streamline Curvature and Buoyancy in Turbulent Shear Flow," J. Fluid Mech., Vol. 36, Part 1, pp. 177-191, 1969.
2. Bradshaw, P., Effects of Streamline Curvature on Turbulent Flow, AGARDograph No. 169, AGARD-AG-169, North Atlantic Treaty Organization (NATO), August 1973.
3. Wilcken, H., "Effect of Curved Surfaces on Turbulent Boundary Layers," NASA TT F-11421, 1967 (translation of Ing.-Arch., Vol. 1, 1930, p. 357).
4. Wendt, F., "Turbulente Stromungen zwischen zwei rotierenden jkon axialen Zylindern, Ing.-Arch., Vol. 4 1933, p. 577.
5. Wattendorf, F.L., "A Study of the Effect of Curvature on Fully Developed Turbulent Flow," Proc. Roy. Soc. A., Vol. 148, 1935, p. 565.
6. Schmidbauer, H., Turbulent Friction Layer on Convex Surfaces, NASA Tech. Memo 791 and ARC No. 2608 (translations of Luftfahrtforsch, Vol. 13, 1936, p. 160.)
7. Wattendorf, F.: personal communication. An internal Goettingen report was prepared by Wattendorf and Maccoll in 1928.
8. Wattendorf, F.: personal communication.
9. Eskinazi, S. and Yeh, H., "An Investigation on Fully Developed Turbulent Flows in a Curved Channel," J. Aero. Sci., Vol. 23, 1956, p. 23.
10. Forthmann, E., Über turbulente Strahlansbreitung, NACA TM 789, 1936 (translation of Ing.-Arch., Vol. 5, 1934, p. 42).
11. Newman, B.G., "The Deflection of Plane Jets by Adjacent Boundaries--Coanda Effect," Boundary Layer and Flow Control, G.V. Lachmann, ed., Vol. 1, Pergamon, London, 1961, p. 232.

12. Bradshaw, P. and Gee, M.T., Turbulent Wall Jets With and Without an External Stream, ARC R. and M. 3252, 1960.
13. Stratford, B.S., Jawor, Z.M., and Smith, M., The Mixing Between Hot and Cold Airstreams in a Centrifugal Field, ARC CP 793, 1965.
14. El-Taher, R.M., "Similarity in Ventilated Wall Jets," AIAA-82-4030, AIAA Journal, Vol. 20, No. 2, February 1982.
15. El-Taher, R.M., "Experimental Investigation of Curvature Effects on Ventilated Wall Jets," AIAA Journal, Vol. 12, No. 11, November 1983.
16. Wood, D.H. and Bradshaw, P., "A Turbulent Mixing Layer Constrained by a Solid Surface. Part 1, Measurements Before Reaching the Surface," J. Fluid Mech., Vol. 122 pp. 57-89, 1982.
17. Wang, C., "The Effects of Curvature on Turbulent Mixing Layers," UMI Dissertation Information Service, 1984.
18. Oertel and Kirchantz (1979) In: "Recent Developments in Theoretical and Experimental Fluid Mechanics" (U. Müller, K.G. Roesner and B. Schmidt, eds.), Springer-Verlag, Berlin, 355-366.
19. Oertel (1982) In: "Flow Visualization II" (W. Merzkirch, ed.), Hemisphere, Washington, 71-76.
20. Minardi, J.E., von Ohain, H.P., Newman, R.K., and Lawson, M.O., "Feasibility Analysis of the Internal Bypass Monorotor Engine," AFWAL-TR-86-2057, November 1986.
21. Minardi, J.E., von Ohain, H.P., and Lawson, M.O., "Internal Bypass Gas Turbine Engines With Blade Cooling," Patent pending.